Polarimetric Analysis of Black Hole X-ray Binaries

Vladislav Loktev (University of Turku)

1st CDY workshop on "Black Hole Flares"

CCA, Flatiron Institute

November 14th 2023, NYC

UNIVERSITY OF TURKU

belliavesha.github.io

Black hole X-ray binaries

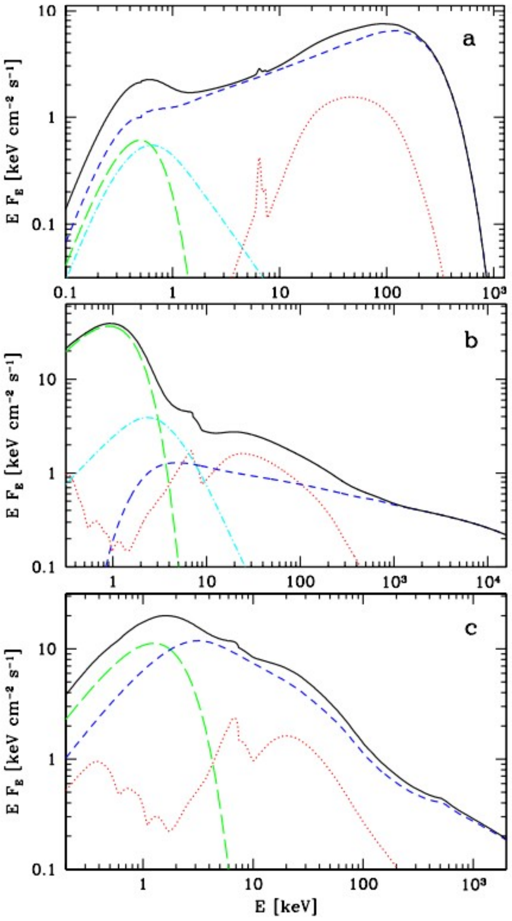

[Zdziarski 2004]

States and spectral components

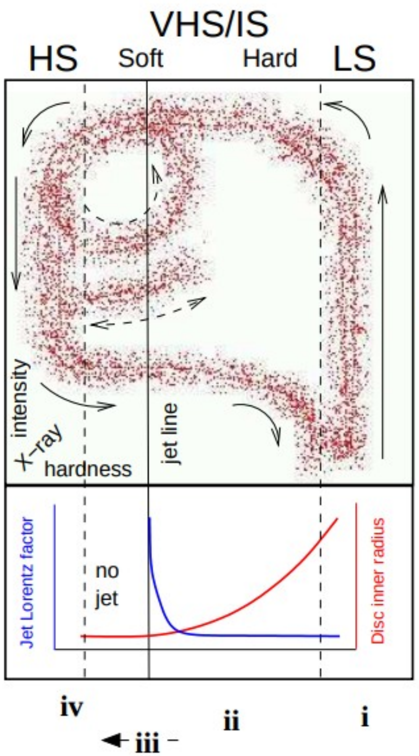

[Remillard & McClintock 2006]

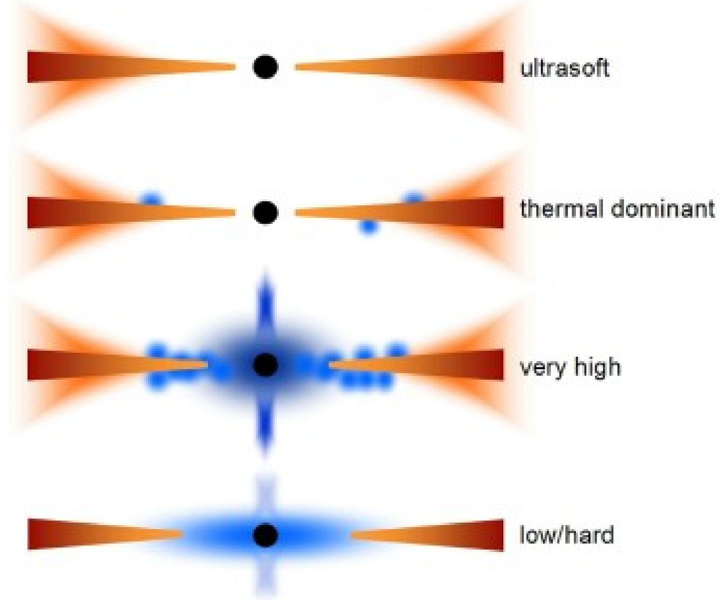

[Done et al. 2007]

X-ray polarization, Comptonisation

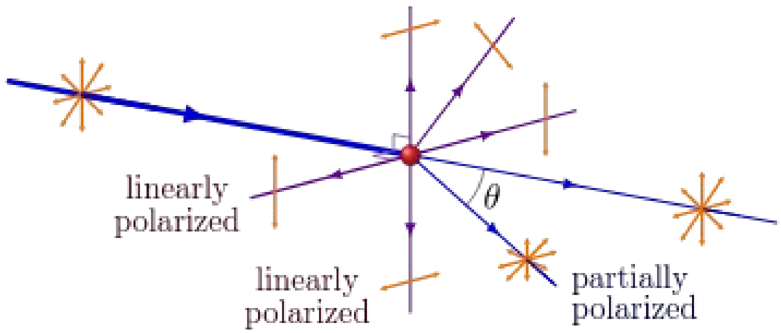

Compton scattering

- Shows the assimetric geometry of the emitting surface

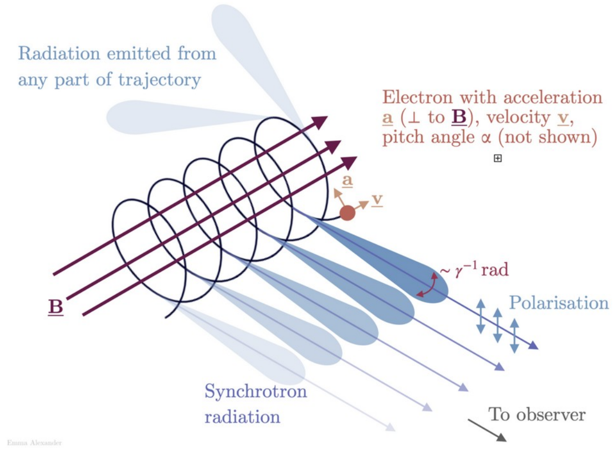

Synchrotron

- Shows the structure of magnetic field structure

BH XRBs with IXPE

High mass

- Cyg X-1 (hard state, soft state)
- Cyg X-3 (low and high flux state)
- LMC X-1 (high soft state)
- LMC X-3 (high soft state)

Low mass

- 4U 1630-47 (high soft state, steep power law)
- 4U 1957+115 (high soft state)
- Swift J1727.8–1613 (hard intermediate)

Extended source

- eastern lobe of SS 433

Cyg X-1

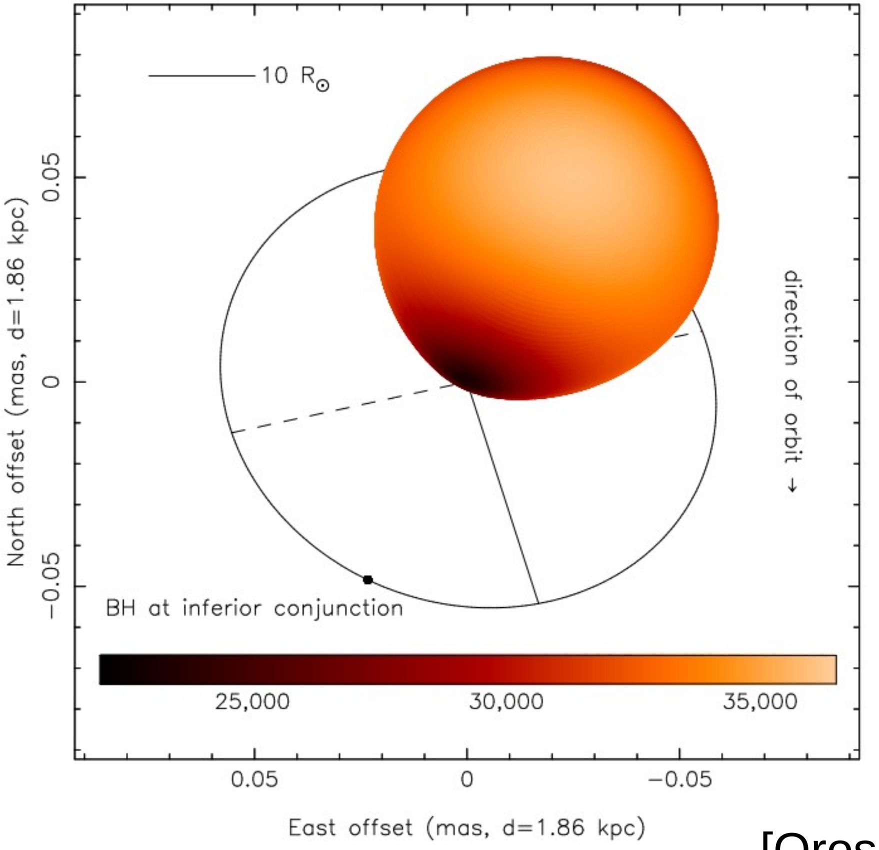

- 21±2 solar-mass black hole in a
- 40±7 solar-mass star
- 5.6 day orbit
- jets have been imaged in the radio band
- i = 27.5^o ± 0.8^o inferred from optical observations

[Orosz et al. 2011]

Cyg X-1

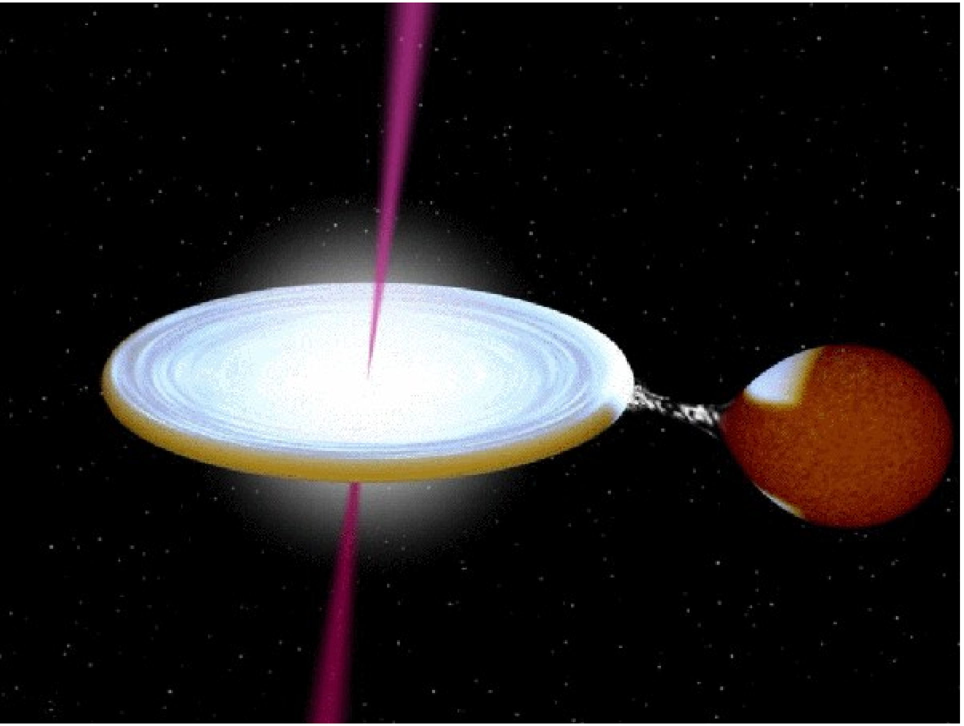

- 21±2 solar-mass black hole in a
- 40±7 solar-mass star
- 5.6 day orbit
- jets have been imaged in the radio band
- $i = 27.5^{o} \pm 0.8^{o}$ inferred from optical observations
- But jet and orbital plane alignment is an assumption

e. g. Jet-orbit misalignment in MAXI J1820+070 [Poutanen et al. 2022]

Cyg X-1

Jet alignment

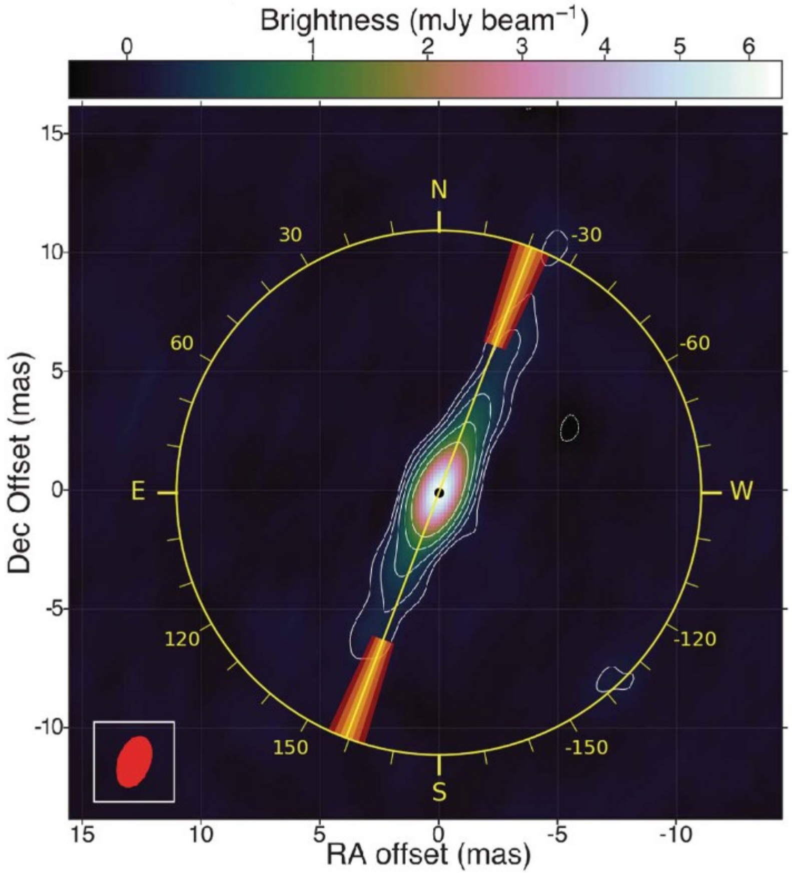

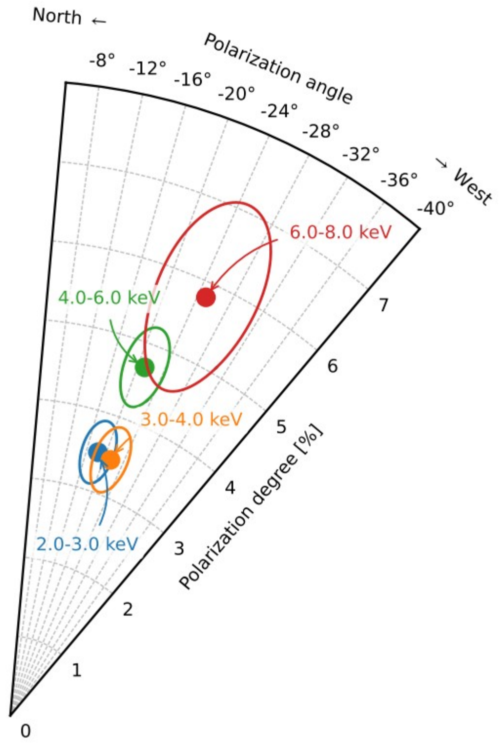

[Krawczynski et al. 2023]

- 20 sigma detection of polarization. Can be resolved into energy bands
- Perfectly aligns with the jet image

Cyg X-1

Corona models

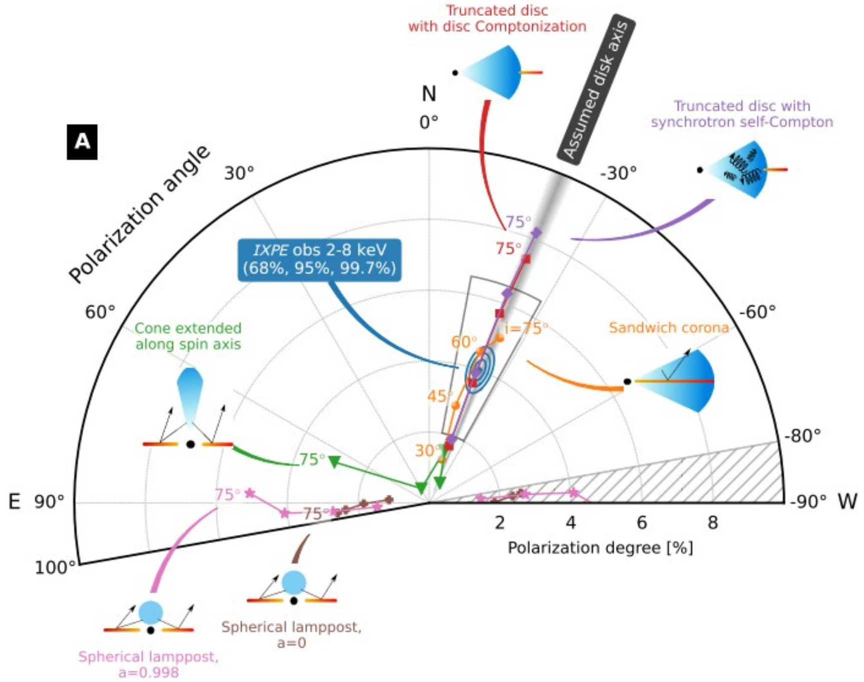

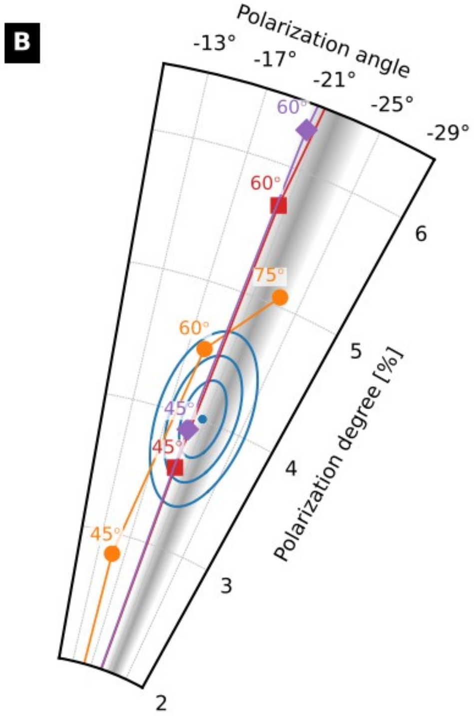

[Krawczynski et al. 2023]

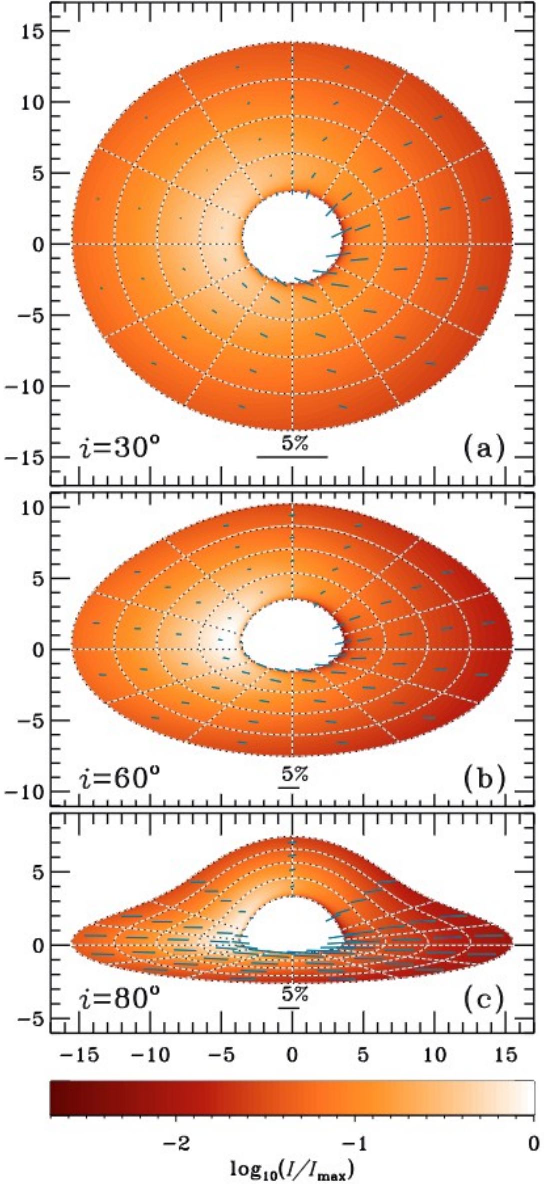

[Loktev et al. 2022]

-
-

Cyg X-1

Warped disk?

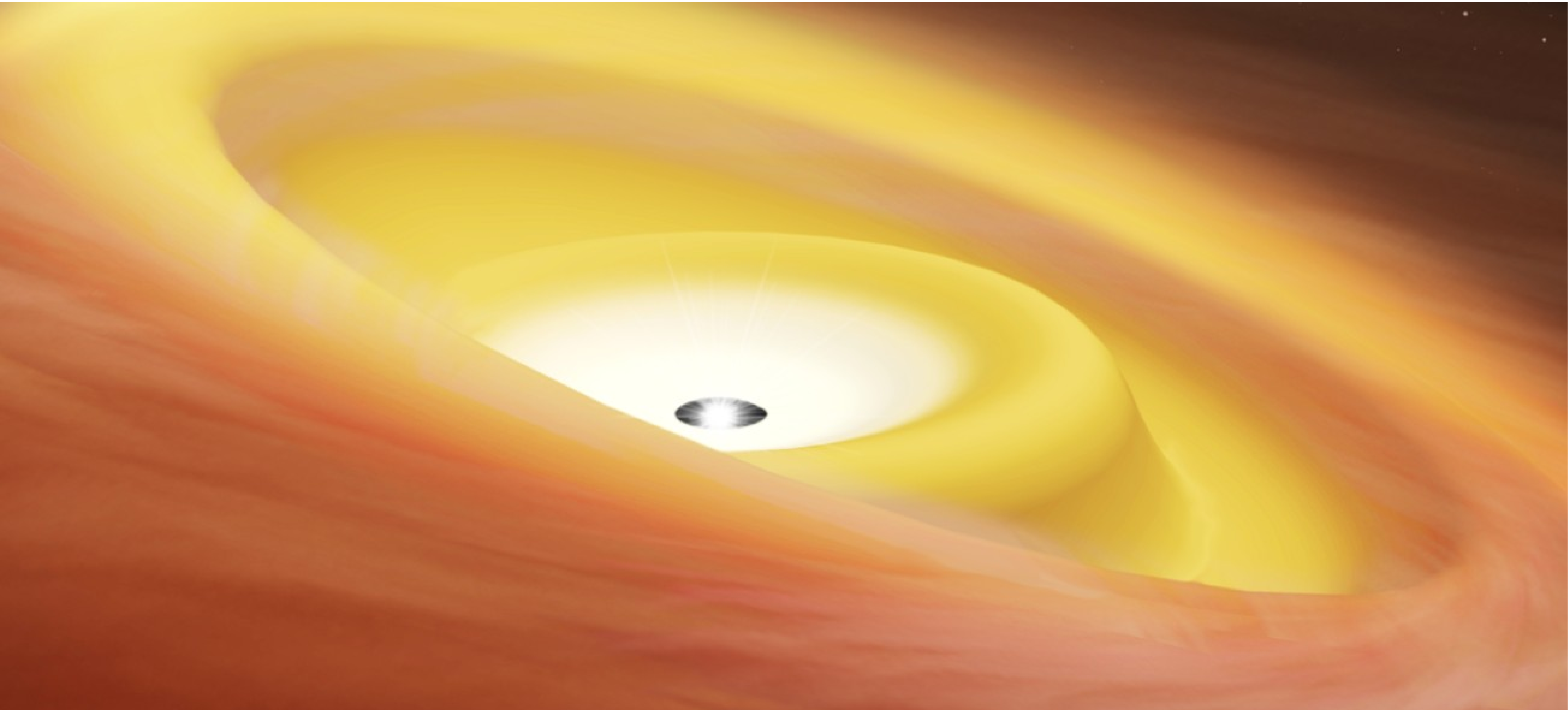

Cyg X-1

Superorbital variability?

Optical

X-ray

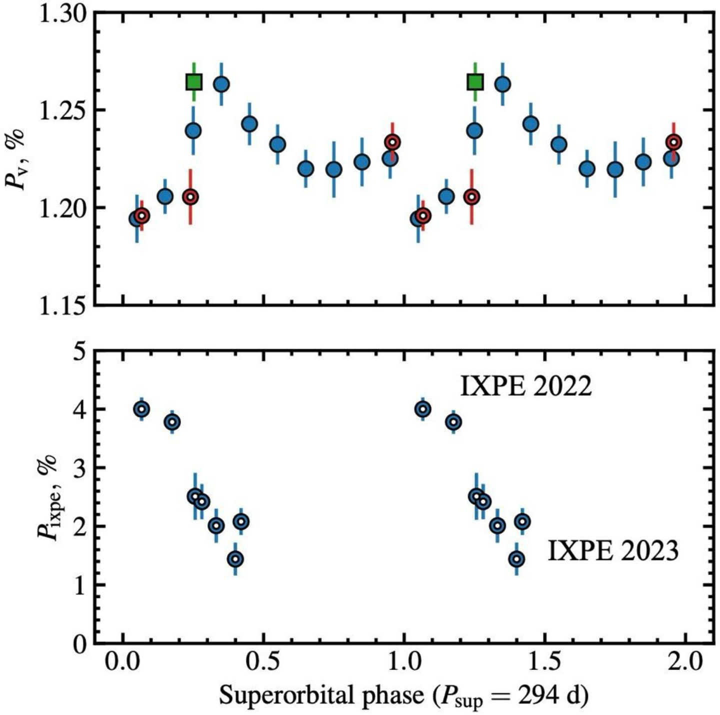

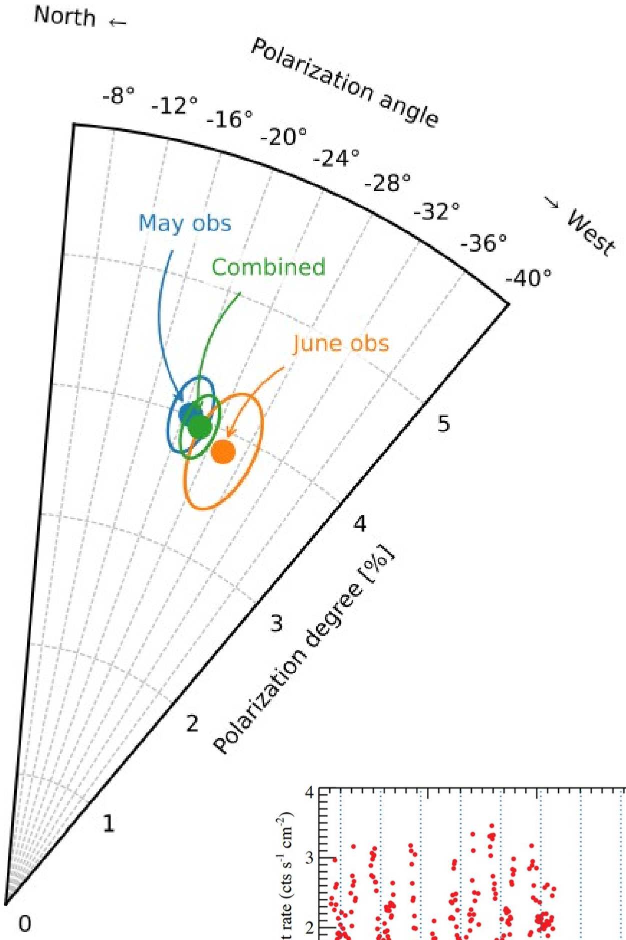

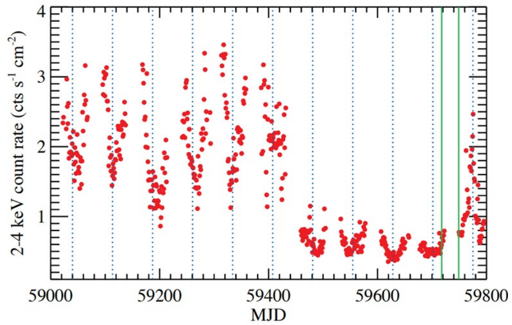

[Krawczynski et al. 2023]

Cyg X-1

Windy accretion?

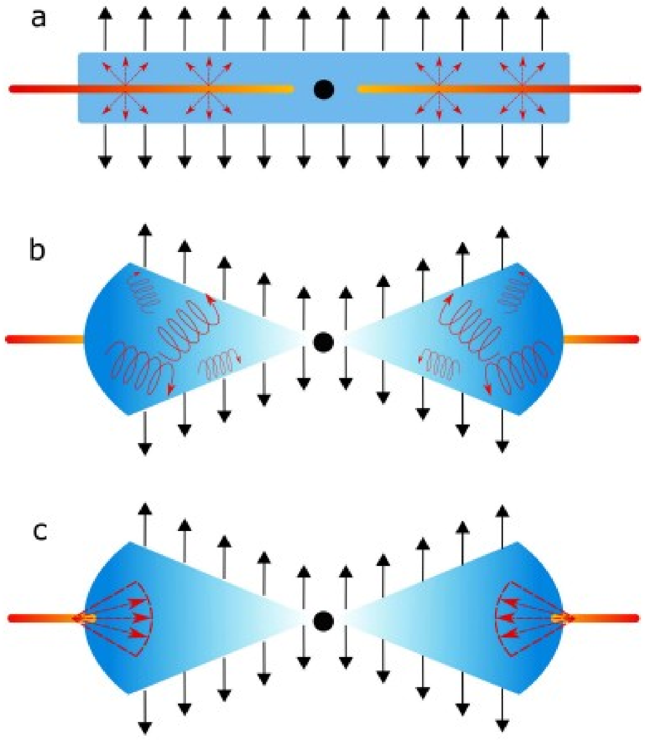

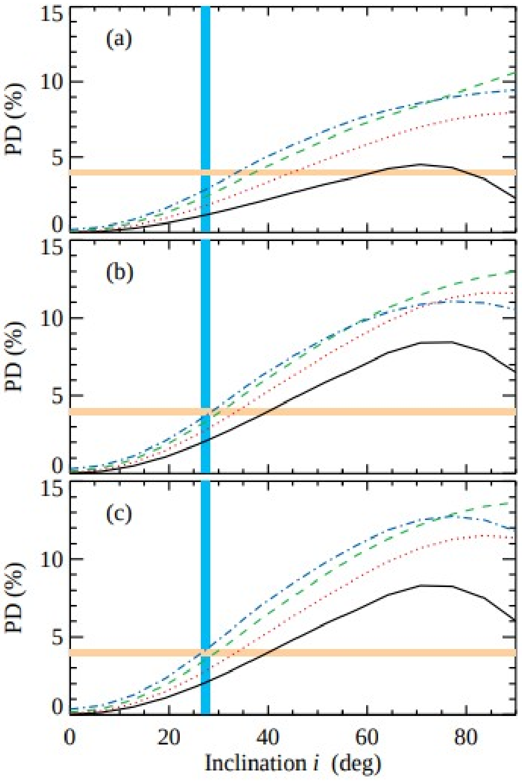

Relativistic (~0.6 c) vertical motion of the emitting surface can increase the observed polarization degree due to relativistic aberration

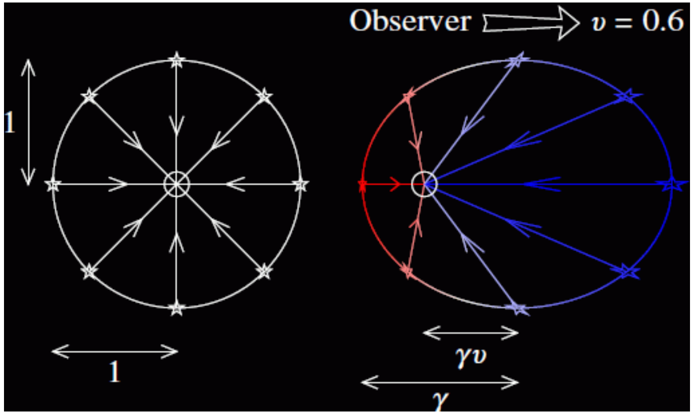

[Poutanen 2023]

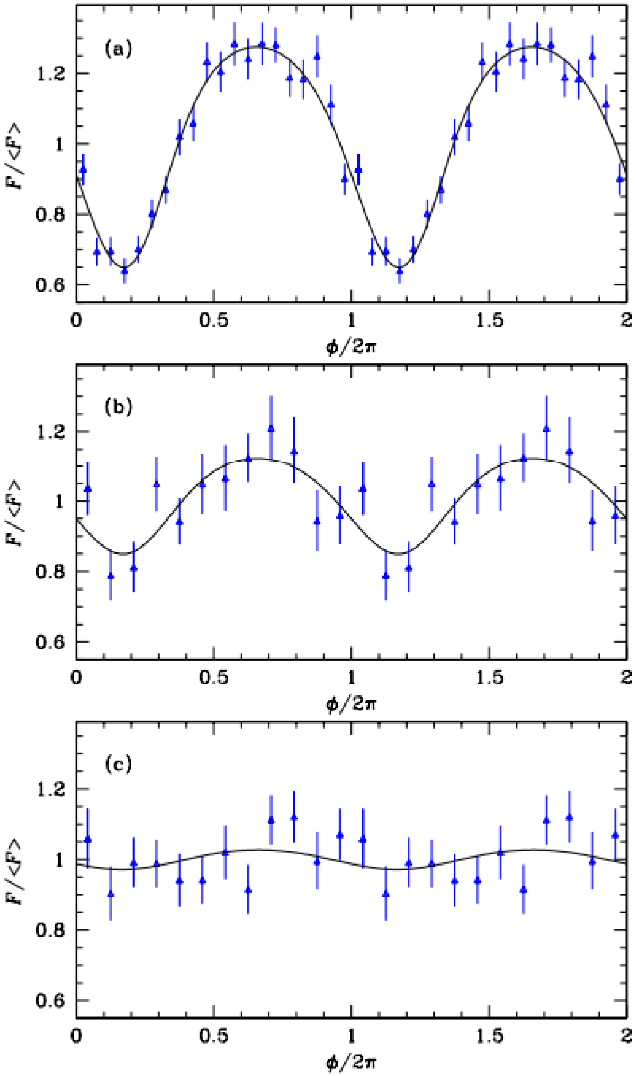

Cyg X-1

Orbital modulation (radio)

- strong orbital modulation of the radio flux is due to absorption of the jet emission by the stellar wind of the donor
- observed delays show the jet is inclined with respect to the binary axis ≈ 16^o–33^o

[Zdziarski et al. 2023]

Cyg X-1

Orbital modulation (optical)

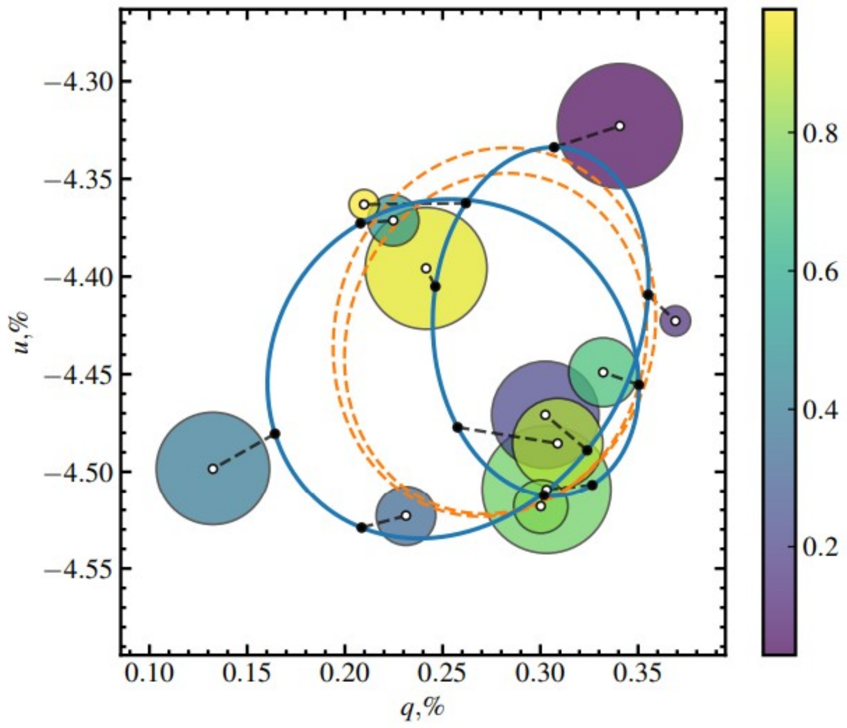

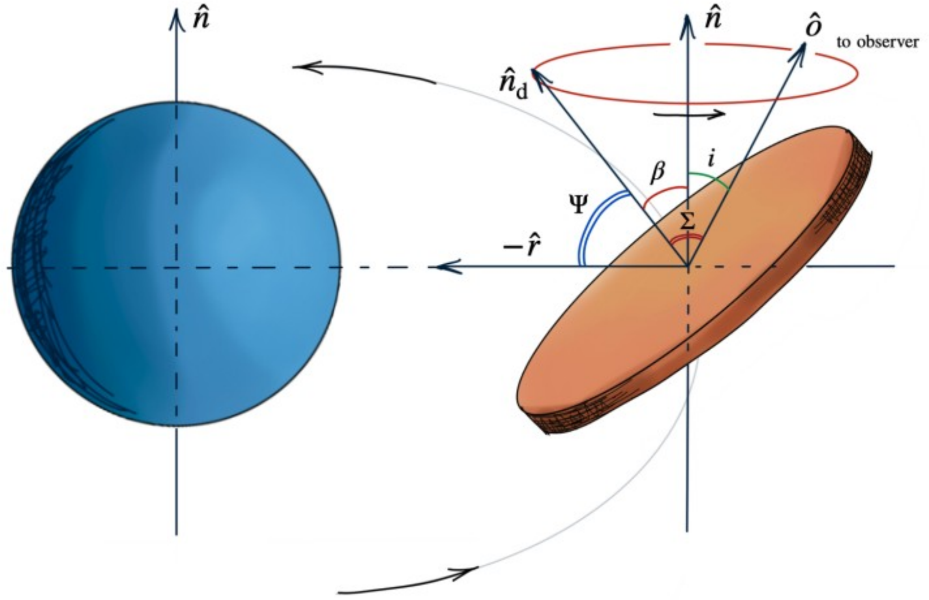

- The misalignment of $\beta = 15^o$-30^o is necessary to reproduce the orbital behavior of the optical polarization.

[Kravtsov et al. 2023]

Cyg X-1

Soft state X-ray polarization

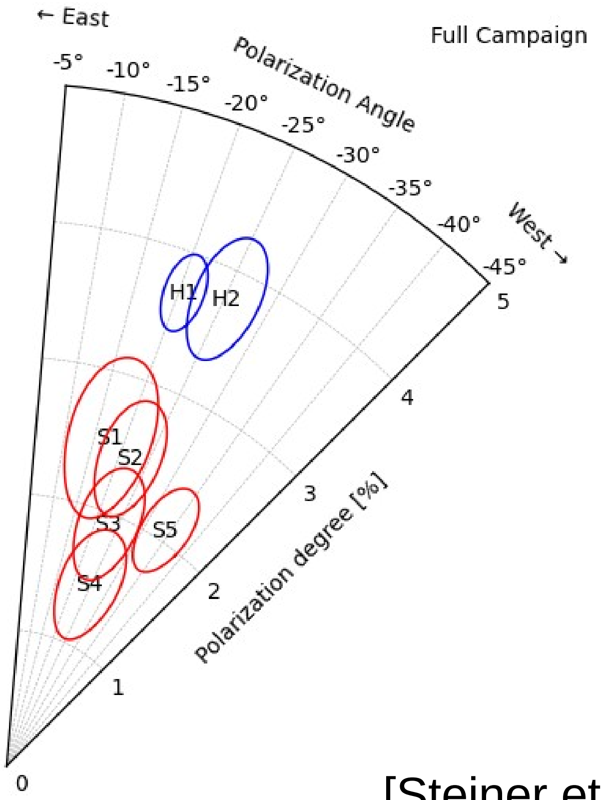

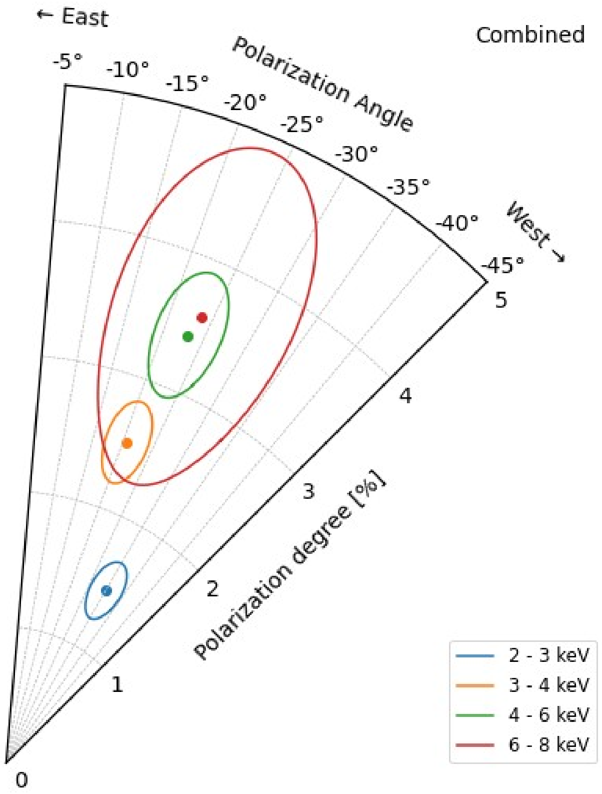

[Steiner et al. in prep]

Cyg X-1

Summary

- Evidence of jet-disk-orbit misalignment
  - High polarization degree
  - Optical and radio modulations
- While also evidences of alignment
  - Radio jet aligns with X-ray PA
  - No superorbital PD dependence

4U 1630-37

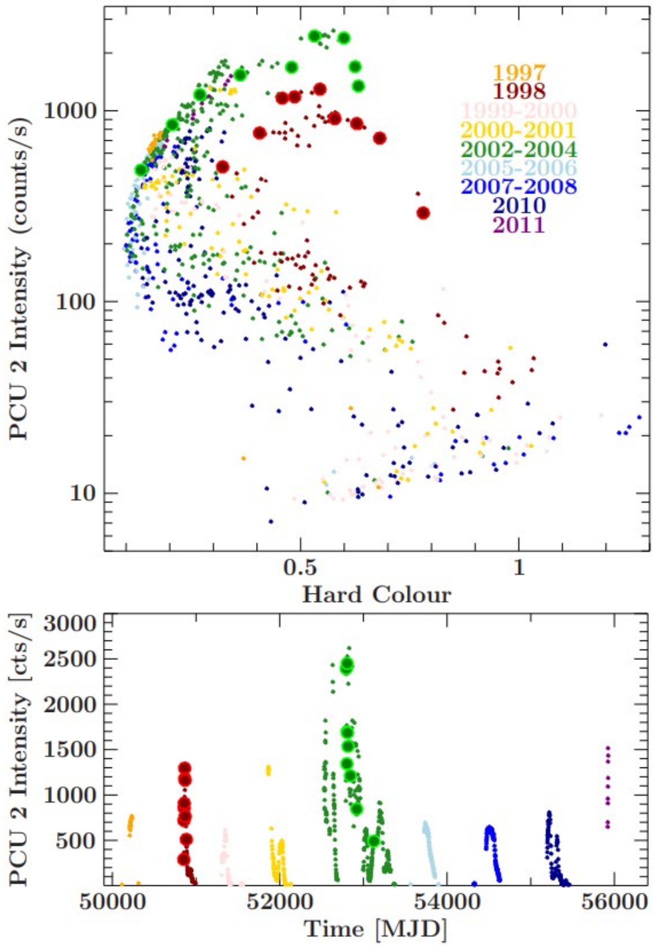

- Low mass XRB, transient
- one of the most active BHBs to have been observed.
- Short hard states
- Distance ~11.5 kpc [Kalemci et al. 2018]
- Mass, inclination angle – unconstrained (estimated high, dips but not eclipses)
- Orientation – unresolved

4U 1630-37

Polarization

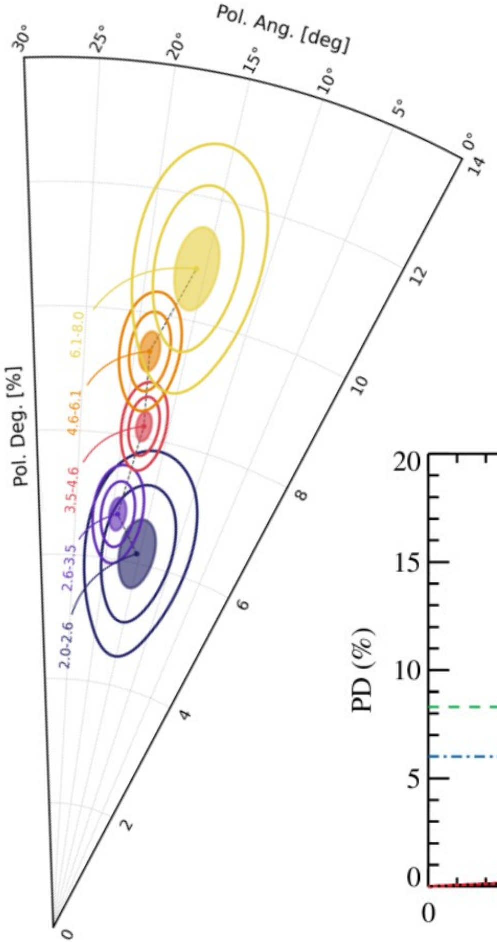

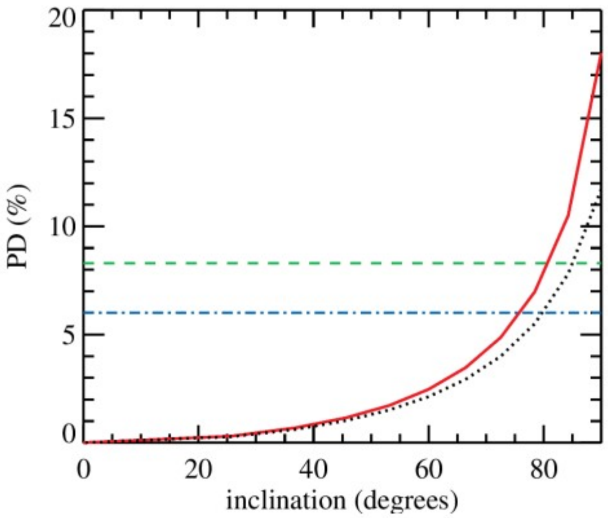

[Ratheesh et al. 2023]

- Polarization is much higher than predicted from a standard thin disk model
- polarisation degree and position angle are 8.32 ± 0.17% and 17.8^{o} ± 0.6^{o}
- Linear dependence of PD, rises with energy, no dependence of PA

4U 1630-37

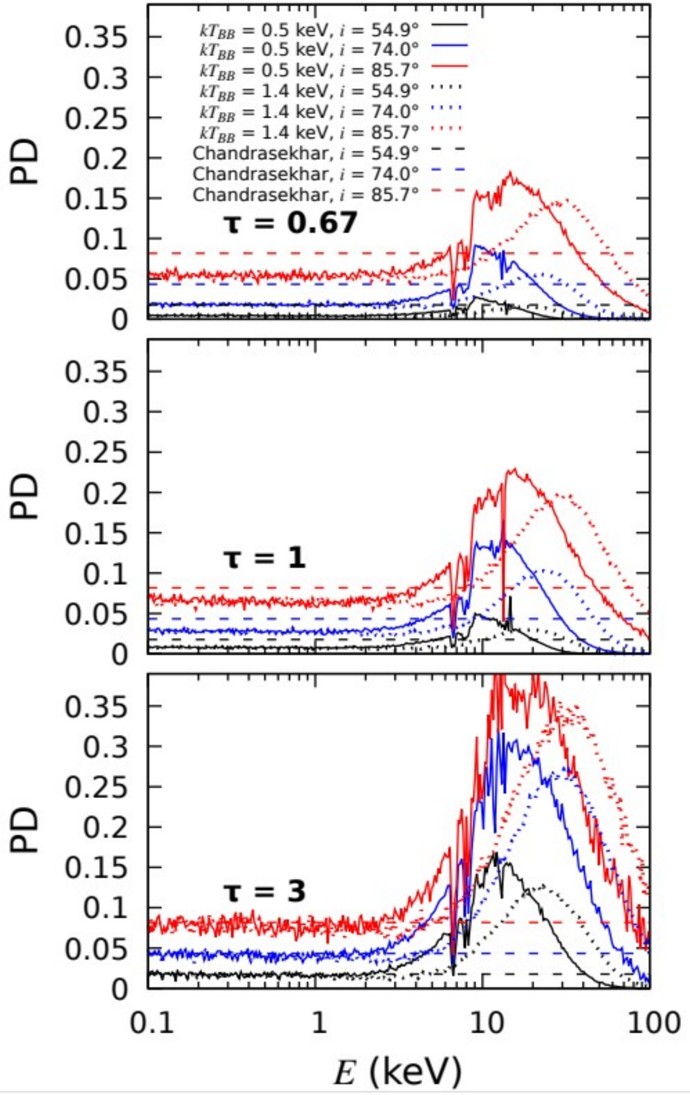

[Ratheesh et al. 2023]

Atmosphere model

- First observation: soft state, powerlaw contribution 3%
- A highly-ionised atmosphere (absorption effects) is considered to explain high PD and energy dependence

4U 1630-37

Polarization

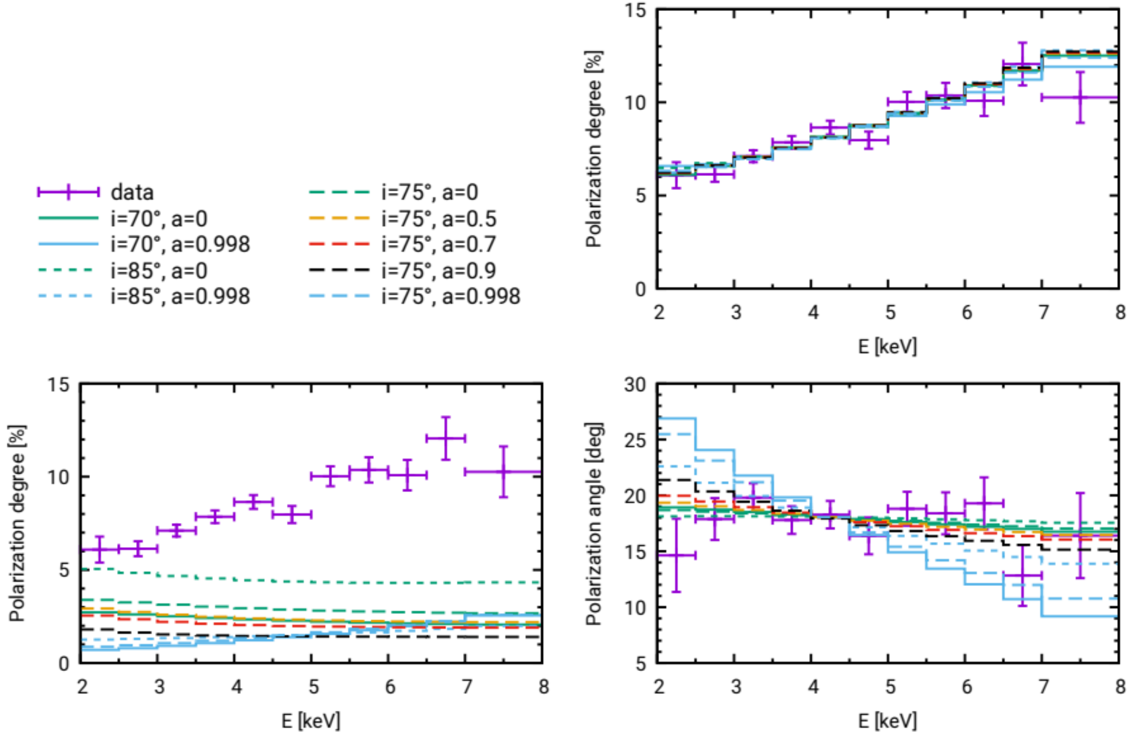

- When we include this extra effect into the partially-ionised slab model, we can explain the observed PD and PA (right panels)
- a low black hole spin (a < 0.5)
- a highly-ionised atmosphere with large optical depth (τ ∼ 7)
- outflowing perpendicular to the accretion disc with a velocity 0.5 c

[Ratheesh et al. 2023]

[Loktev et al. 2023, in prep]

4U 1630-37

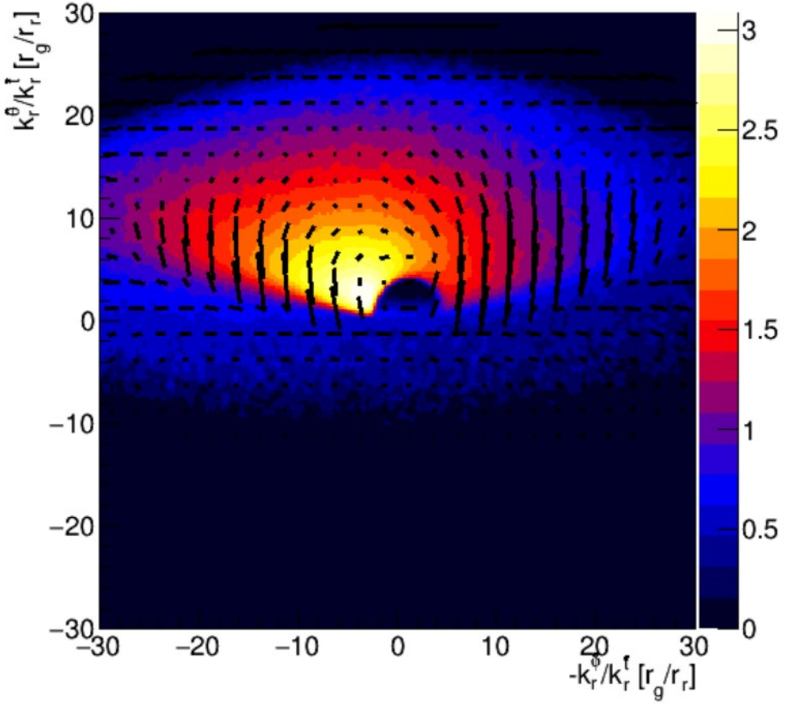

H = h/r= 0.5

[Ratheesh et al. 2023]

Polarization from a thick disk

- PD rises with energy
- No parameter combination that achieves PD as high as the observed ones.

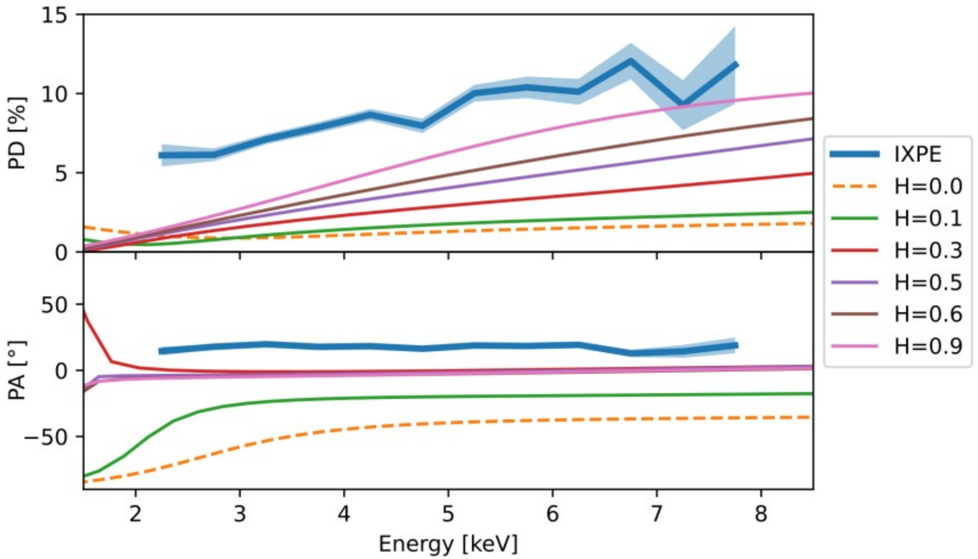

4U 1630-37

Second observation

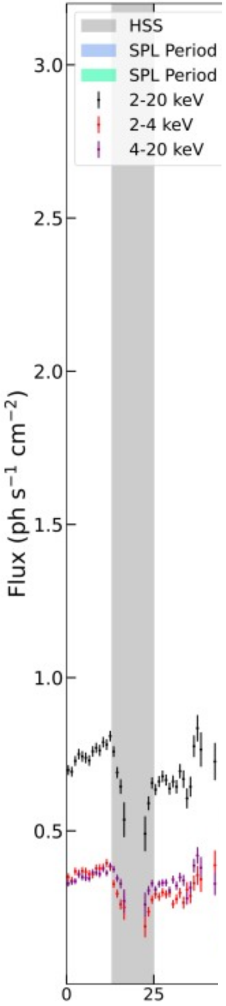

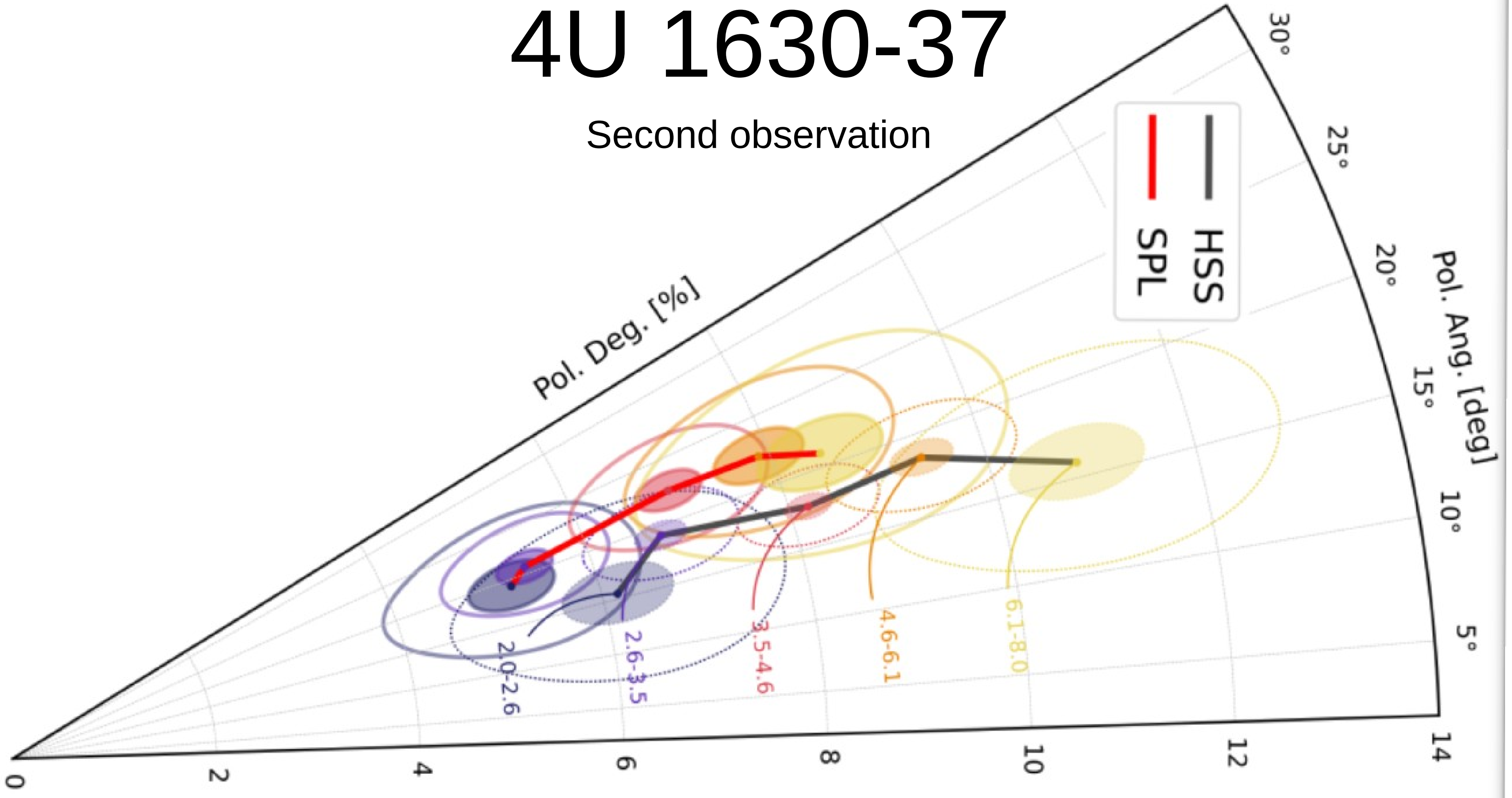

[Rodriguez-Cavero et al. 2023]

4U 1630-37

Summary

- Even higher polarization than in Cyg X-1, in soft state
- Explained with low spin black hole and large τ outflowing ionized atmosphere
- Polarization properties are similar before and after the state transition

Cyg X-3

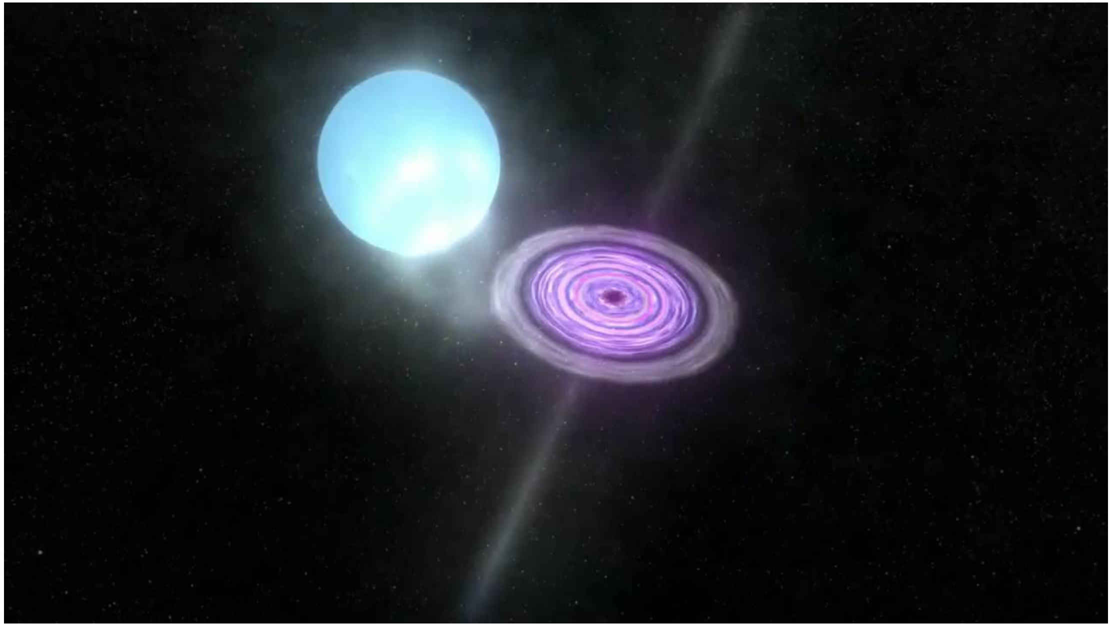

[NASA visualization, Walt Feimer]

- D = 7.4 ± 1.1 kpc
- Close system with a WR star (unique)
- i = $38^o \pm 12^o$ (depends on assumd mass of the star); or $30^o \pm 1^o$ [Antokhin et al. 2022]
- Jet inclination <14^o [Miller-Jones et al. 2004]
- Orbital period 4.8 h
- One of the few galactic sources with gamma detections
- First IXPE observation: October 2022

Cyg X-3

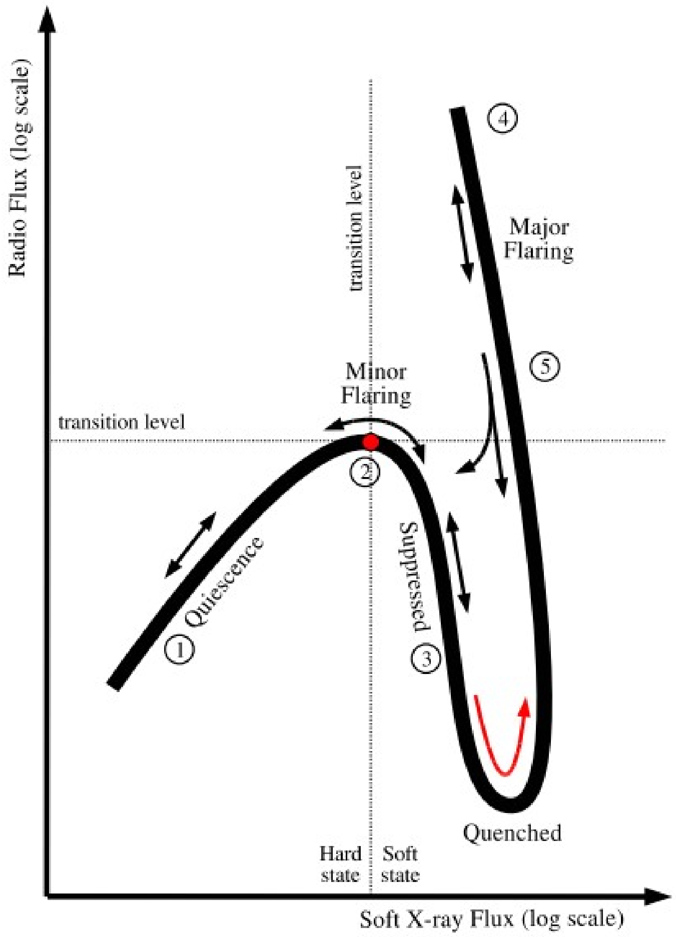

[Veledina et al. 2023]

States

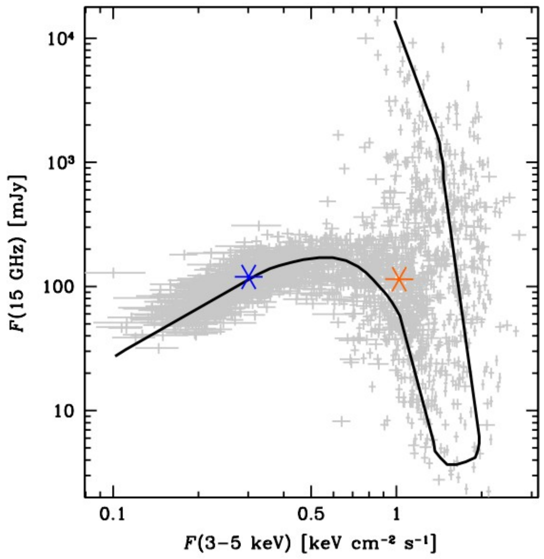

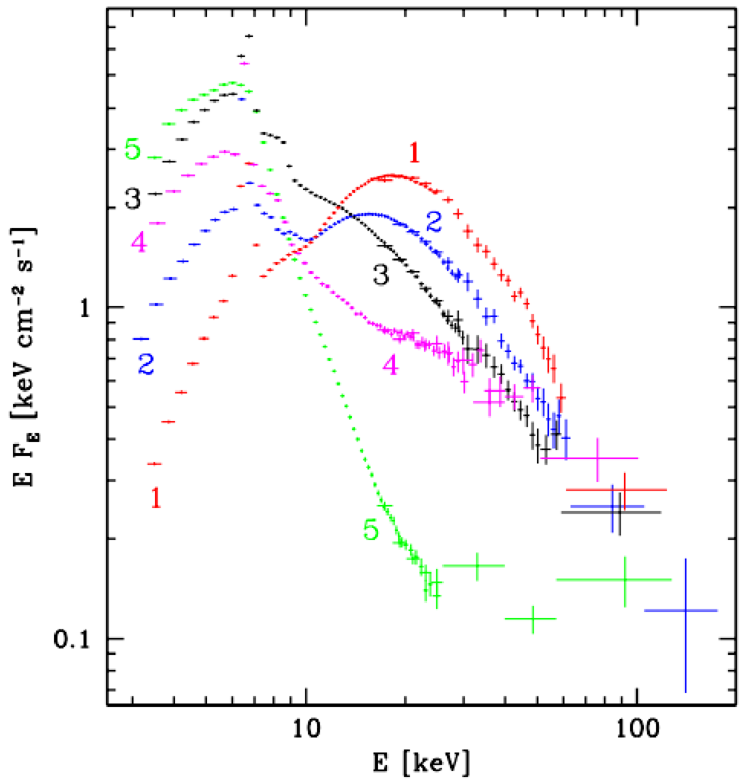

- Quiescent can be explaied in a number of ways

➢ soft + absorption;

➢ hard + truncated cold disk

➢ Incident + reflection

Cyg X-3

Averaged polarization

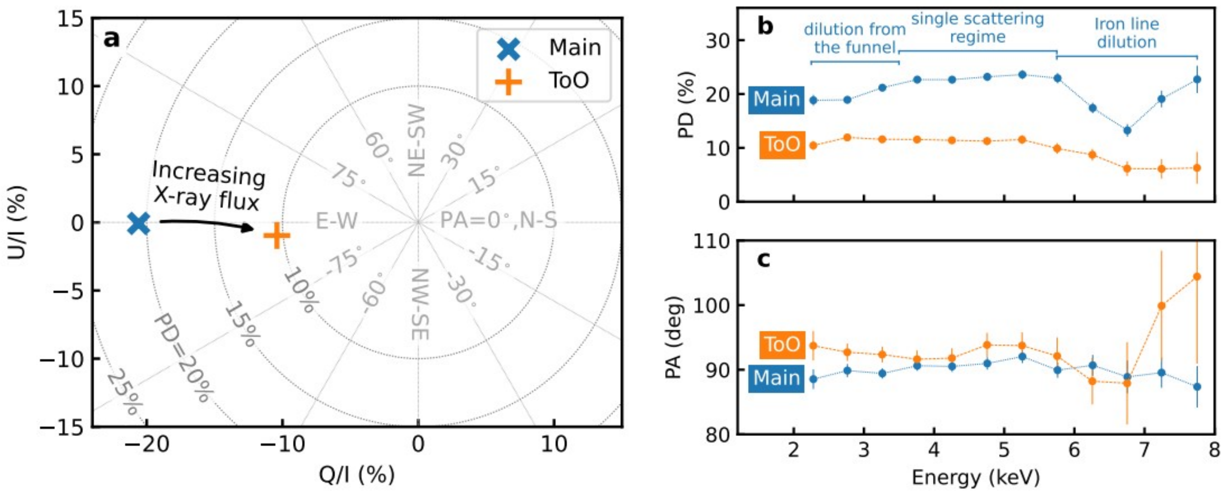

- High polarization fraction with no dependence on energy is a sign of a single scattering as a source of polarization
- PA is orthogonal to the position angle of the radio ejections

[Veledina et al. 2023]

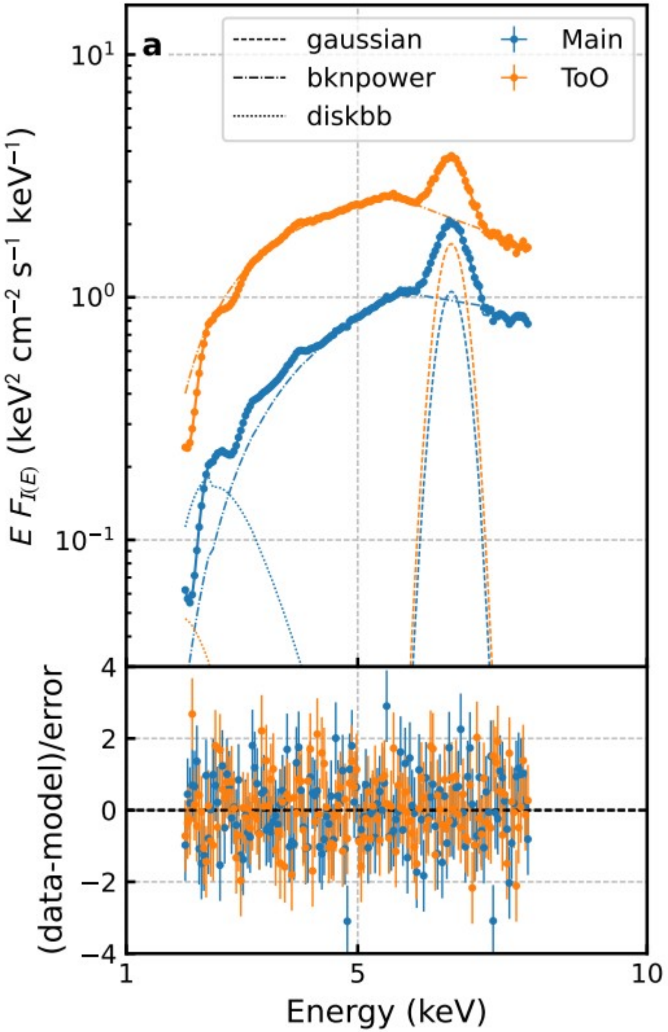

Cyg X-3

- broken power-law component typical for ULXs

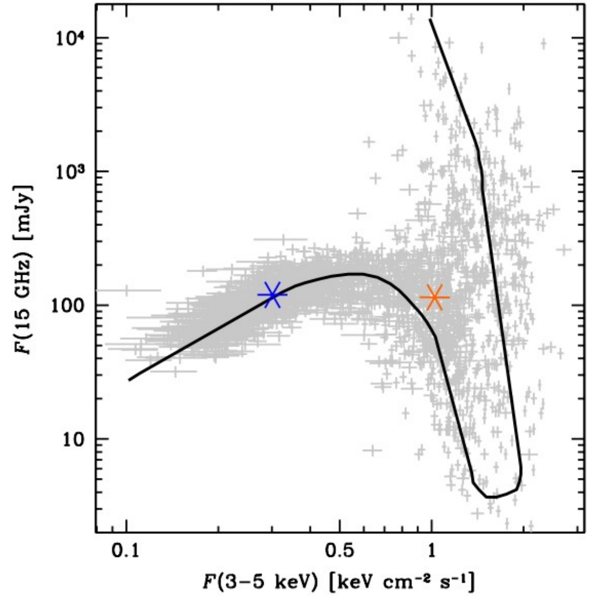

Second observation Dec 2022

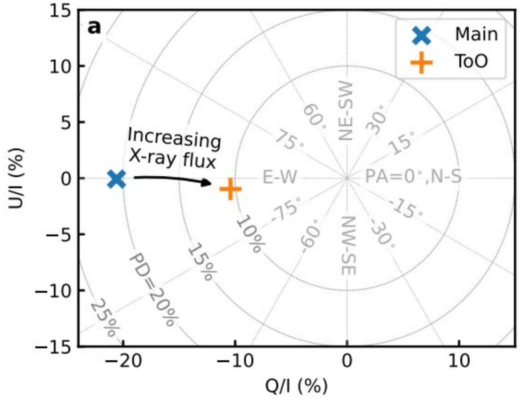

[Veledina et al. 2023]

Cyg X-3

Folded polarization

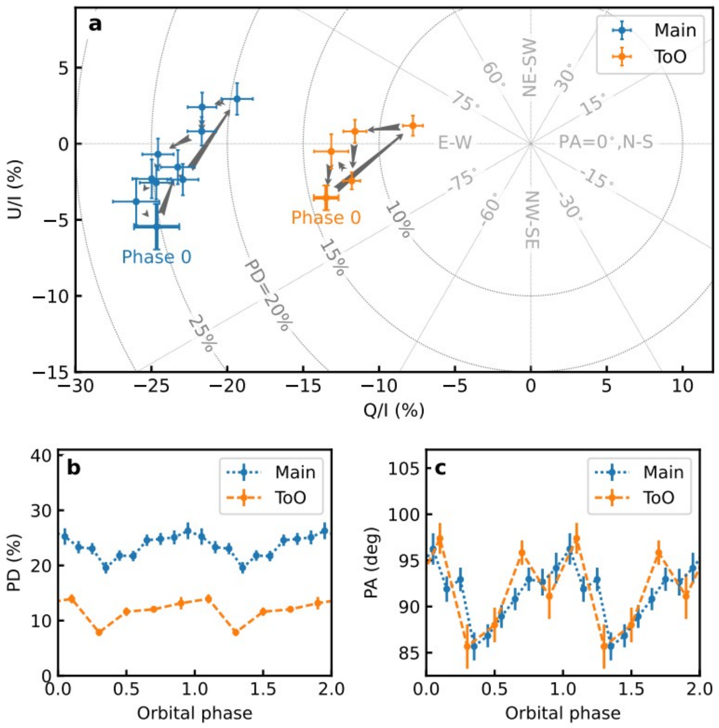

- “**Single-**loop” and **high PD** orbital variations rool out scattering off the wind
- Variations may be explained by reflection off a bow shock

[Veledina et al. 2023]

Cyg X-3

Funnel geometry

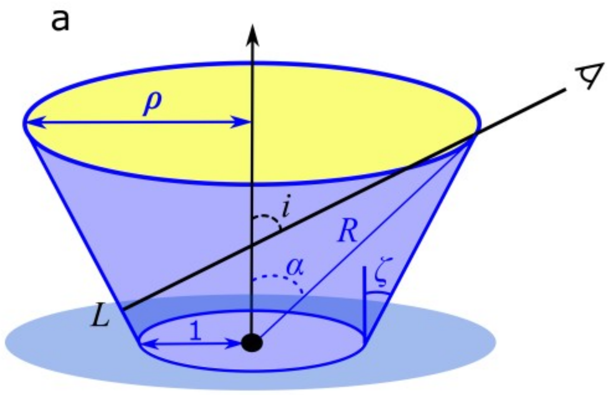

[Veledina et al. 2023]

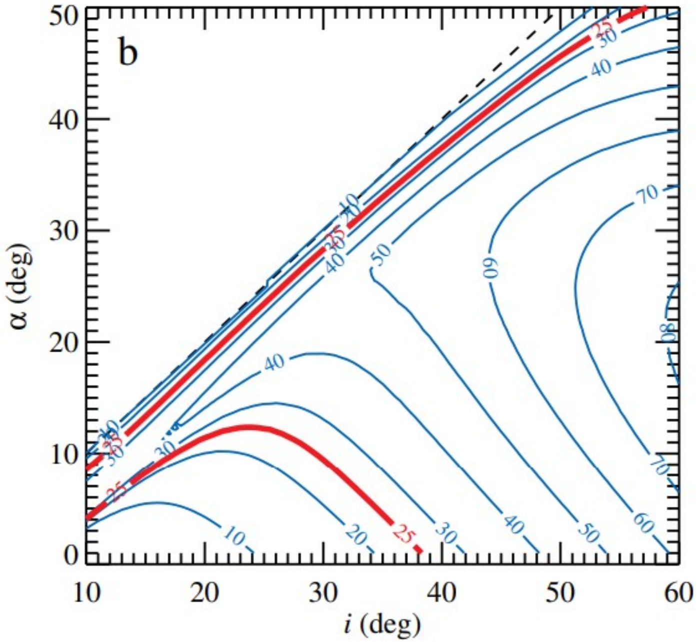

- Proposed funnel geometry, we see X-rays reflected from optically thick outflow
- The geometry of the funnel is constrained from polarization degree (high funnel)

Cyg X-3

Funnel geometry

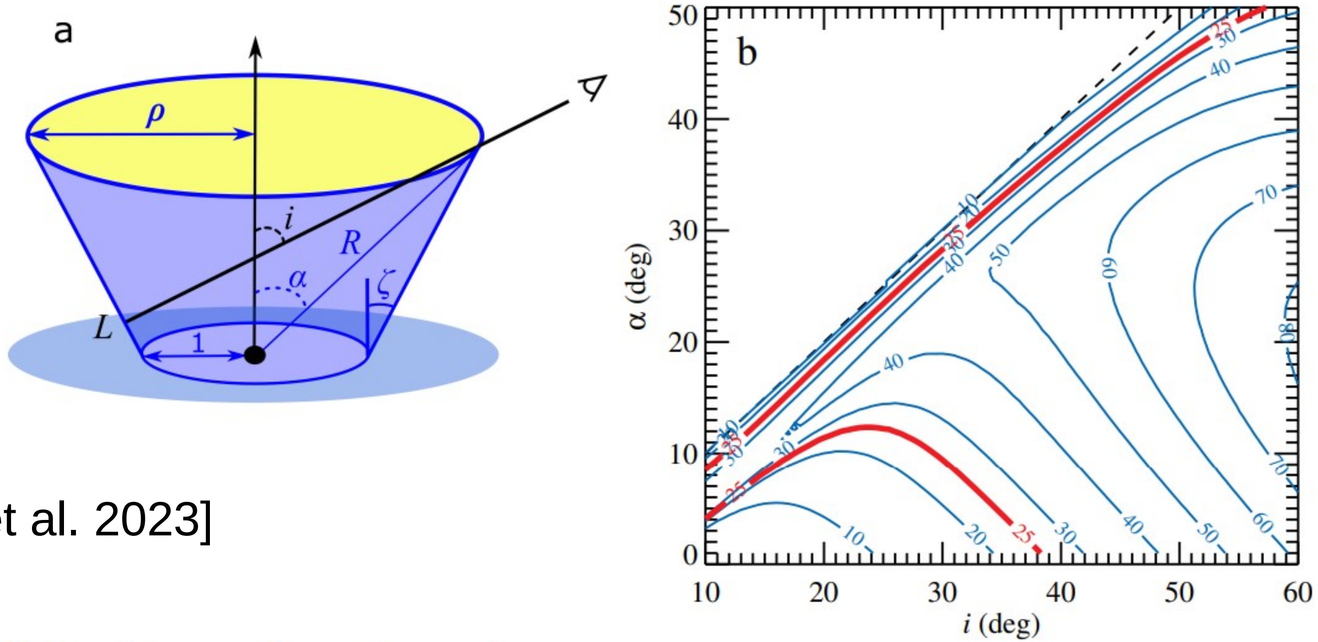

[Veledina et al. 2023]

$$L_{\rm X,bol} = \frac{4\pi D^2 f_{\rm bol} F_{\rm unabs}}{a}\left(1 + \frac{\Omega_{\rm ULX}}{\Omega_{\rm refl}}\right)$$

- Eddington limi is exceeded even for a black hole of 20 solar masses

Cyg X-3

Summary

- High polarization (25%) due to single scattering reflection
- Single-loop orbital variations
- PD change between observations, funnel parameters might have changed
- A hidden supper-luminous source
  - the accretion rate might be lower when the source appears brighter

Modeling the polarization spectrum

1. Geometry of the system
2. Local emission at the disk
3. Gravitational redshift and Doppler boosting
4. Light bending and rotation of the polarization frame

Modeling the polarization spectrum

Geometry

- Assume thin equatorial disk
- For a soft state disk around a Kerr BH, the inner radius of the disk depends on the spin parameter

Redshift

- For the emissionfrom from the equatorial plane of the BH, the SR and GR redshift is computed analytically

Local emission

- The radial emission pattern also depends on spin, null hypothesis (and our example) is a standard thin disk described in [Novikov & Thorne (1973)]

- As a simples local atmosphere model we can adopt Chandrasekhar’s electron sattering atmosphere.

Insert your analytically described model here.

Modeling the polarization spectrum

Geometry

- Assume thin equatorial disk
- For a soft state disk around a Kerr BH, the inner radius of the disk depends on the spin parameter

Redshift

- For the emissionfrom from the equatorial plane of the BH, the SR and GR redshift is computed analytically

Local emission

- The radial emission pattern also depends on spin, null hypothesis (and our example) is a standard thin disk described in [Novikov & Thorne (1973)]

- As a simples local atmosphere model we can adopt Chandrasekhar's electron sattering atmosphere.

$$r_{\rm ISCO} = \frac{1}{2}\left(3 + Z_2 \pm \sqrt{(3 - Z_1)(3 + Z_1 + 2Z_2)}\right)$$

$$Z_1 = 1 + \sqrt[3]{1 - a^2}\left(\sqrt[3]{1 + a} + \sqrt[3]{1 - a}\right)$$

$$Z_2 = \sqrt{3a^2 + Z_1^2}.$$

Modeling the polarization spectrum

Geometry

- Assume thin equatorial disk
- For a soft state disk around a Kerr BH, the inner radius of the disk depends on the spin parameter

Redshift

- For the emissionfrom from the equatorial plane of the BH, the SR and GR redshift is computed analytically

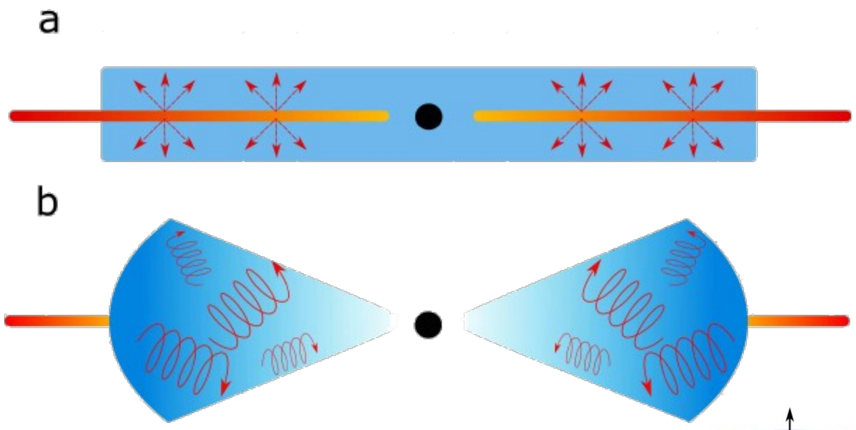

Local emission

- The radial emission pattern also depends on spin, null hypothesis (and our example) is a standard thin disk described in [Novikov & Thorne (1973)]

- As a simples local atmosphere model we can adopt Chandrasekhar’s electron sattering atmosphere.

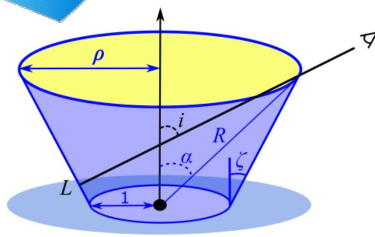

Modeling the polarization spectrum

Geometry

- Assume thin equatorial disk
- For a soft state disk around a Kerr BH, the inner radius of the disk depends on the spin parameter

Redshift

- For the emissionfrom from the equatorial plane of the BH, the SR and GR redshift is computed analytically

Local emission

- The radial emission pattern also depends on spin, null hypothesis (and our example) is a standard thin disk described in [Novikov & Thorne (1973)]

- As a simples local atmosphere model we can adopt Chandrasekhar's electron sattering atmosphere.

$$T_{\rm eff}^4(r) = \frac{3GM\dot{M}}{8\pi\sigma_{\rm SB}R^3} f(r,a) = T_*^4 \frac{f(r,a)}{r^3},$$

$$F_{E'} = \frac{\pi}{f_{\rm col}^4} B_{E'}(f_{\rm col} T_{\rm eff})$$

$$a_{\rm es}(\zeta') = \frac{60}{143}(1 + 2.3\cos\zeta' - 0.3\cos^2\zeta')$$

$$p_{\rm es}(\zeta') = 0.1171 \frac{1 - \cos\zeta'}{1 + 3.582\cos\zeta'}$$

Modeling the polarization spectrum

Geometry

- Assume thin equatorial disk
- For a soft state disk around a Kerr BH, the inner radius of the disk depends on the spin parameter

Redshift

- For the emissionfrom from the equatorial plane of the BH, the SR and GR redshift is computed analytically

Local emission

- The radial emission pattern also depends on spin, null hypothesis (and our example) is a standard thin disk described in [Novikov & Thorne (1973)]

- As a simples local atmosphere model we can adopt Chandrasekhar's electron sattering atmosphere.

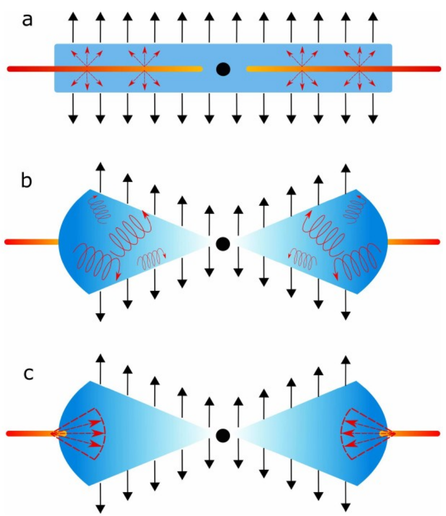

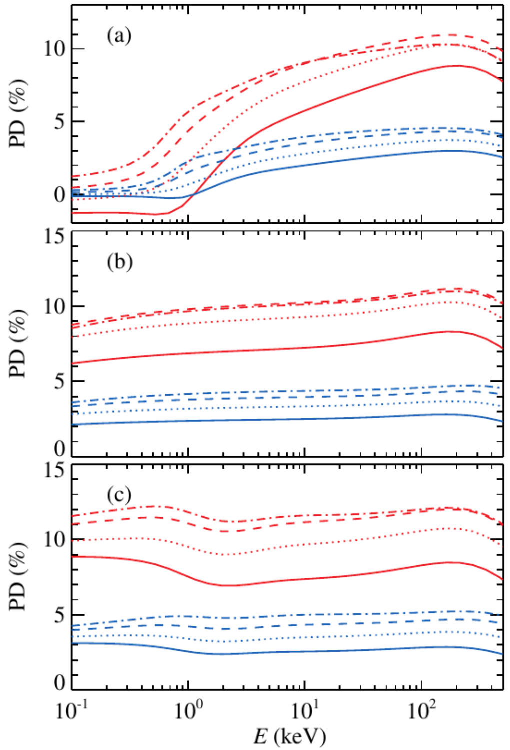

Modeling the polarization spectrum

Geometry

- Assume thin equatorial disk
- For a soft state disk around a Kerr BH, the inner radius of the disk depends on the spin parameter

Redshift

- For the emissionfrom from the equatorial plane of the BH, the SR and GR redshift is computed analytically

$$\beta = \frac{\mathcal{F}}{\mathcal{B}\sqrt{\mathcal{D}}}\sqrt{\frac{1}{2r}}$$

$$g = E/E' = \gamma\left[\mathcal{X} + \mathcal{Y}\beta + (\mathcal{X}\beta + \mathcal{Y})\cos\xi'\right]$$

where

$$\mathcal{X} = \sqrt{\mathcal{D}/\mathcal{A}},$$

$$\mathcal{Y} = a/\sqrt{4r^4\mathcal{A}},$$

$$\mathcal{A} = 1 + (r+1)\frac{a^2}{4r^3}.$$

$$\mathcal{B} = 1 + \frac{a}{\sqrt{8r^3}},$$

$$\mathcal{D} = 1 - \frac{1}{r} + \frac{a^2}{4r^2},$$

$$\mathcal{F} = 1 - \frac{a}{\sqrt{2r^3}} + \frac{a^2}{4r^3}.$$

Local emission

- The radial emission pattern also depends on spin, null hypothesis (and our example) is a standard thin disk described in [Novikov & Thorne (1973)]
- As a simples local atmosphere model we can adopt Chandrasekhar's electron sattering atmosphere.

Modeling the polarization spectrum

Geometry

- Assume thin equatorial disk
- For a soft state disk around a Kerr BH, the inner radius of the disk depends on the spin parameter

Redshift

- For the emissionfrom from the equatorial plane of the BH, the SR and GR redshift is computed analytically

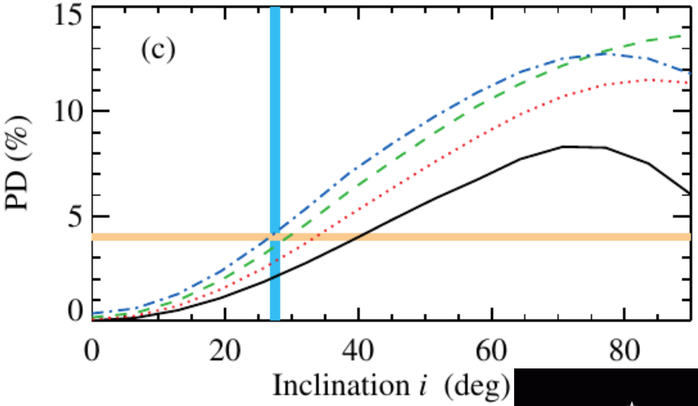

Local emission

- The radial emission pattern also depends on spin, null hypothesis (and our example) is a standard thin disk described in [Novikov & Thorne (1973)]

- As a simples local atmosphere model we can adopt Chandrasekhar's electron sattering atmosphere.

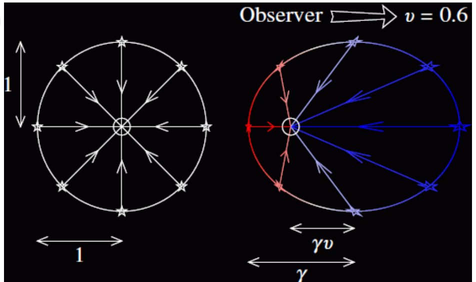

Model: Light bending (Kerr)

The Kerr metric

$$(g_{ab}) = \begin{pmatrix} 1 - \frac{2Mr}{\rho^2} & 0 & 0 & \frac{2Mra\sin^2\theta}{\rho^2} \\ 0 & -\frac{\rho^2}{\Delta} & 0 & 0 \\ 0 & 0 & -\rho^2 & 0 \\ \frac{2Mra\sin^2\theta}{\rho^2} & 0 & 0 & -\sin^2\theta\left(r^2 + a^2 + \frac{2Mra^2\sin^2\theta}{\rho^2}\right), \end{pmatrix}$$

Solving geodesic equations,

$$\frac{\mathrm{d}u^a(\lambda)}{\mathrm{d}\lambda} = -\Gamma^a_{bc}u^b u^c + f^a$$

Simple!

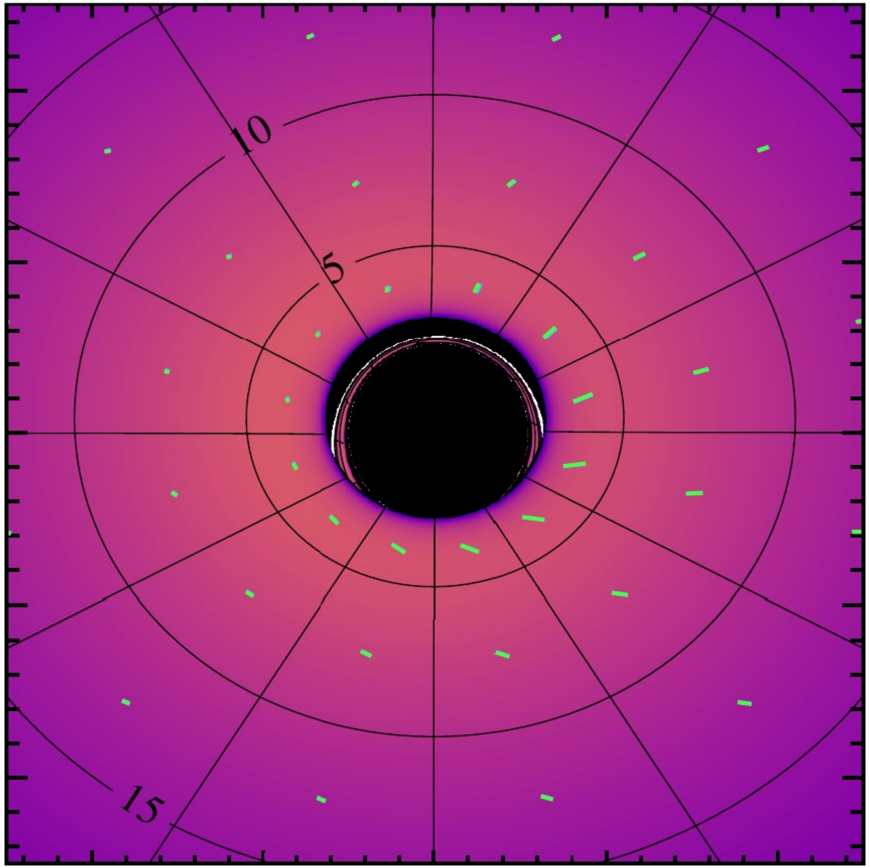

Model: Light bending (Kerr)

$$\frac{du^a(\lambda)}{d\lambda} = -\Gamma^a_{bc} u^b u^c + f^a$$

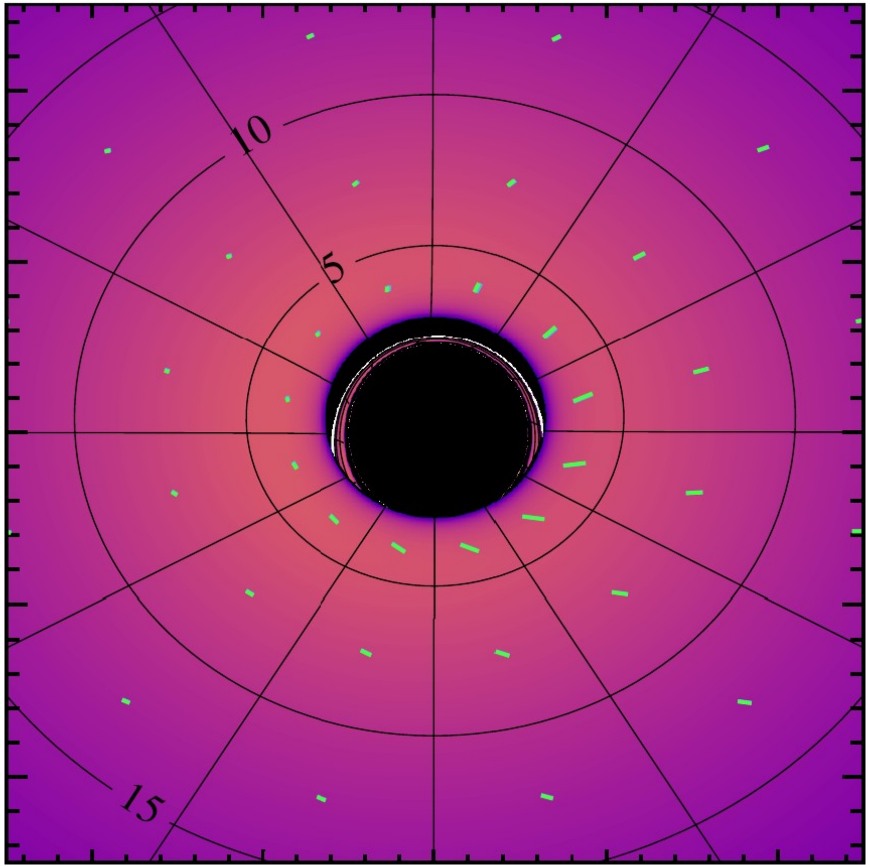

- We trace the geodesics from the observer **back** to the system
- There are **no analytical** solution to the geodesic equation. (slow)
- The result trajectories in the Kerr metric are **non-planar** due to frame-dragging.
- They are the most different from the zero-spin case at the very vicinity to the BH.

Model: Light bending (Schwarzschild)

- The trajectories in the Schwarzschild metric are **planar**
- We do not compute the full trajectory but **explicitly** define the emission angle at the disk.
- We have **analytical** expressions and very good one-line approximation of the light bending
- The PA rotation is also expressed analytically (fast)

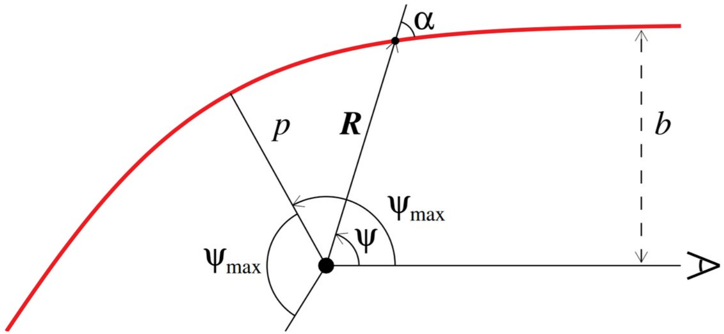

$$\psi(R,\alpha) = \int_R^\infty \frac{\mathrm{d}r}{r^2}\left[\frac{1}{b^2} - \frac{1}{r^2}\left(1 - \frac{R_S}{r}\right)\right]^{-1/2}$$

$$x = (1-u)y\left(1 + \frac{u^2y^2}{112} - \frac{e}{100}uy(\ln(1-y/2) + y/2)\right),$$

where $x = 1 - \cos\alpha$, $y = 1 - \cos\psi$, and $u = 2/r$.

[Poutanen, J. 2020]

Comparing our method with the numerical ray-tracing

*using ARCMANCER [Pihajoki et. al. 2018]

Comparison: at ISCO

- PA rotation (χ^{tot}) and local emission angle (ζ') as a function of azimuth at the ISCO for different BH spins and iclinations.
- The spin are a = 0.2, 0.5, 0.8
- Inclinations are **30°**, **60°**, **80°.**
- The discrepancy between the methods is only significant for the light coming from the disk behind the BH, where the features are shifted by the Kerr frame-dragging

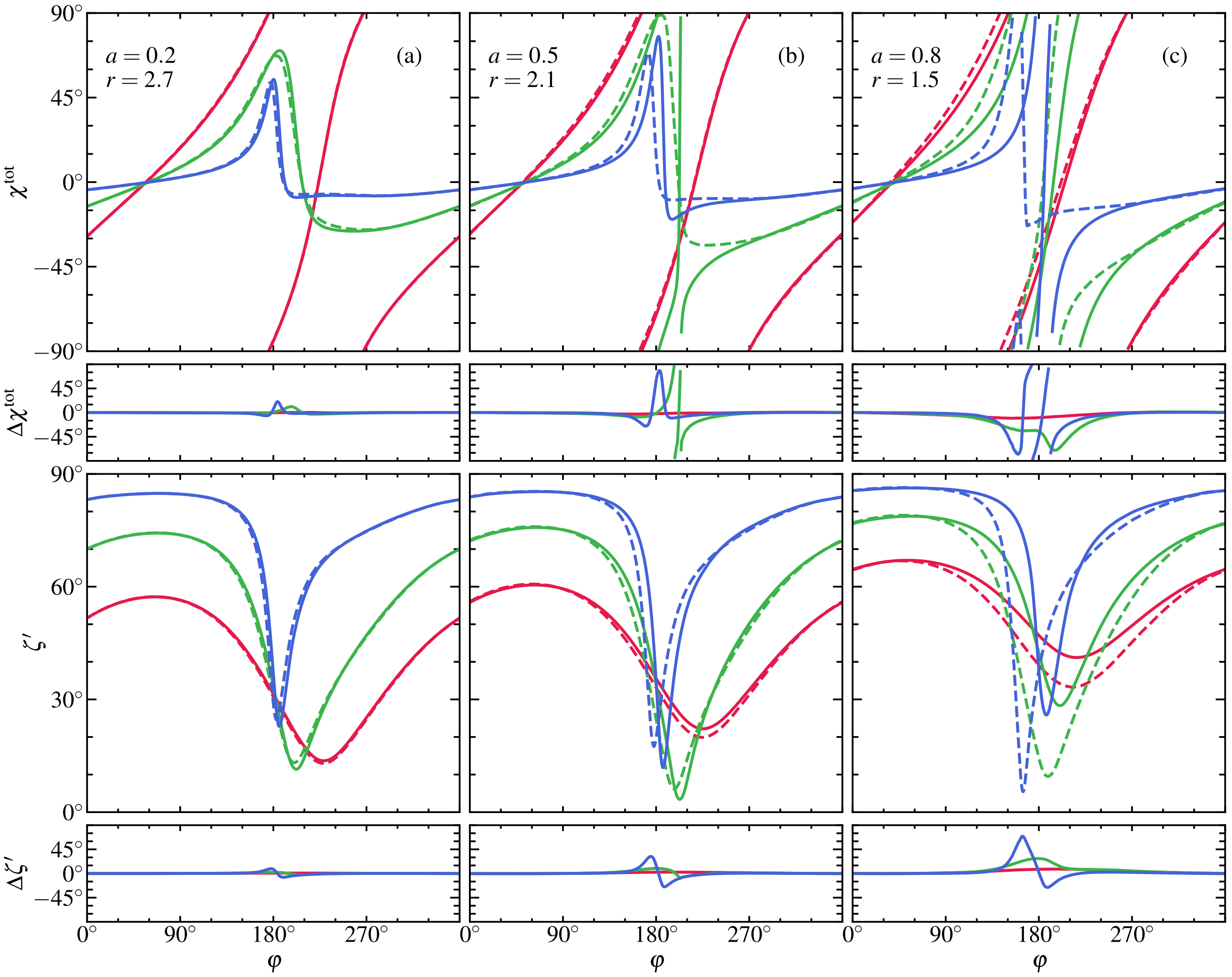

Comparison: wider rings

- PA rotation (χ^{tot}) and local emission angle (ζ’) as a function of azimuth at different distances from the BH
- The spin is 0.8,
- At r = $2R_S$, $3R_S$, $5R_S$
- Inclinations are **30°**, **60°**, **80°.**
- The difference is even less pronounced the further the emitting spot is from the BH

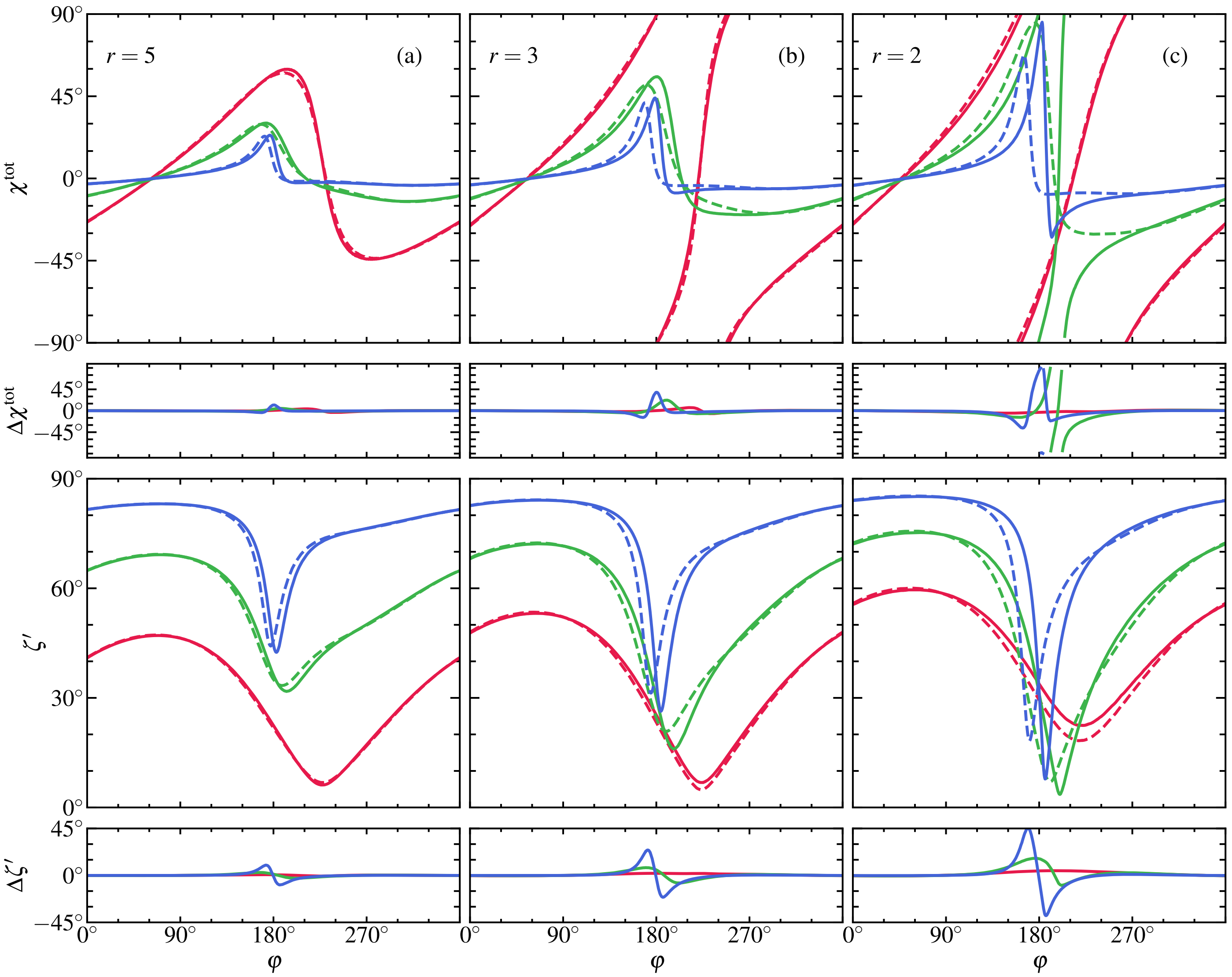

Comparison: imaging

- Images of a thin disk, the inner part **< 12 R_s**
- The spins are a = **0.2, 0.5, 0.8** left to right
- Inclinations are **30°**, **60°**, **80°** top to bottom
- The sticks show polarization computed with **analytical** and **numerical** method, and colormap shows the relative intensity.
- Unless lower right corner, the difference is hard to see.

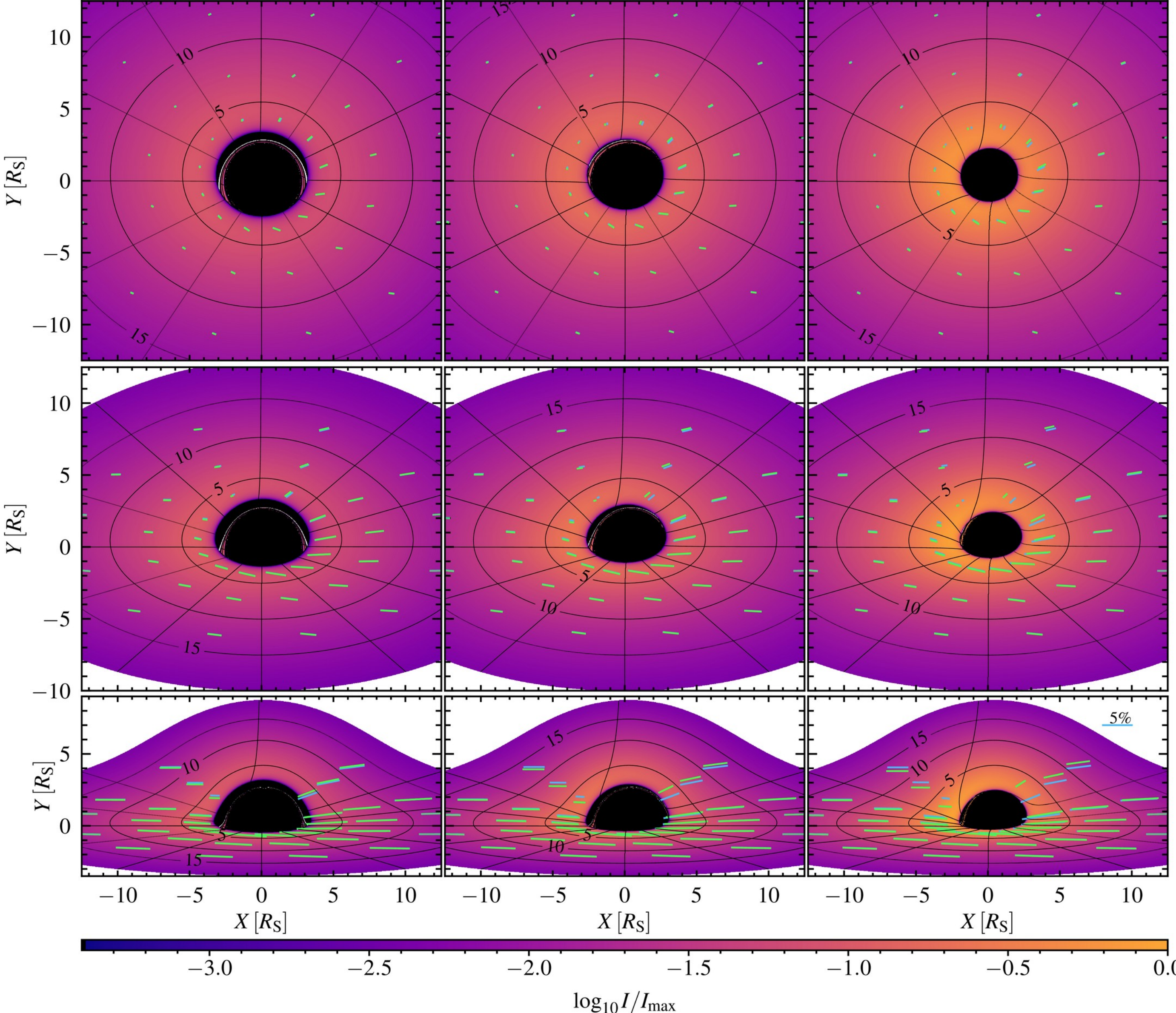

Comparison: spectra

- Polarizaton spectra: relative luminocity (top), PD (middle) and PA (bottom)
- Numerical (dashed) versus analytical (solid)
- The spins are a = **-1**, **0**, **0.5**, **0.8**, **0.94**
- Inclinations are **30°**, **60°**, **80°** left to right.
- For small inclinations th difference is very small.
- For **a > 0.94** the ISCO is below R_S
- In general for **a < 0.8** the results are quite adequate.

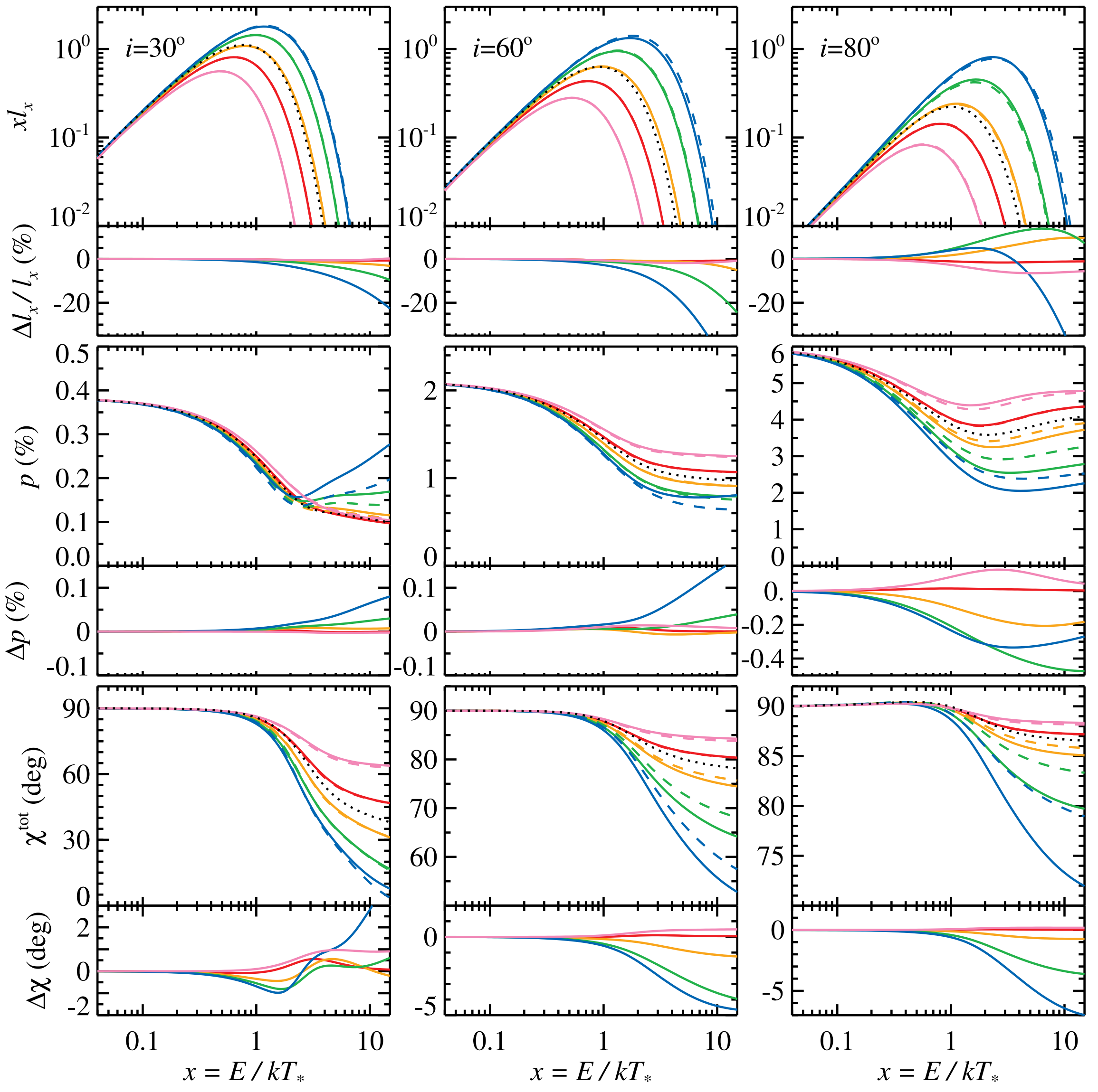

Approximate modeling for Cyg X-1

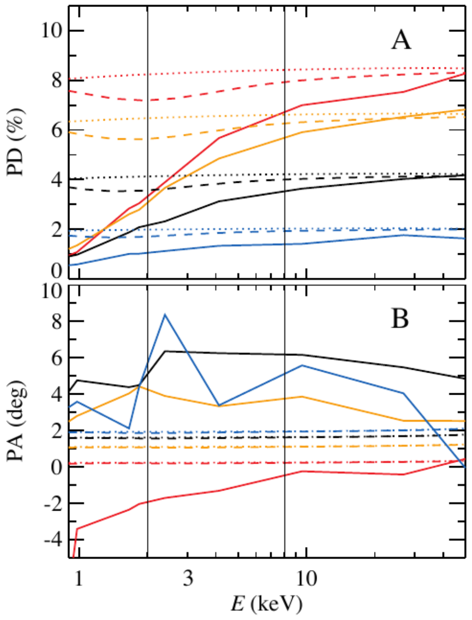

[Krawczynski et al. 2023]

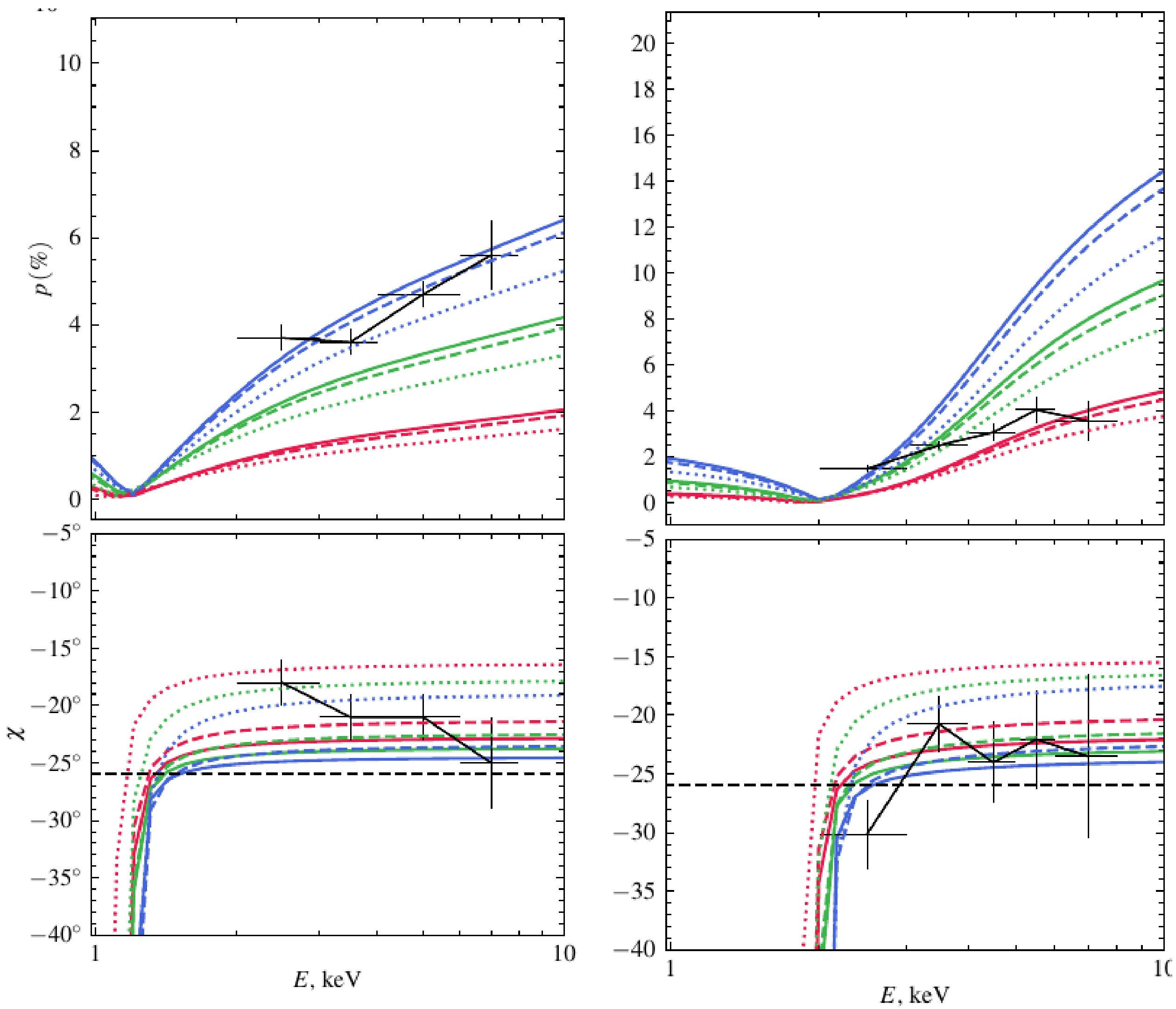

Hard state

Soft state

Conclusions

- BHXRBs is a peculiar class of objects. Sources of this class emit radiation through different mechanisms, many of which are yet to be fully undersood.
- IXPE observations has shed new light on the geomtery of the sources. Polarization measurements helped us to declide some of the existing models and inspired us to produce new ones.
- We developed a fast method of computing polarization spectra from Kerr BH XRBs leveraging the Schwarzschild approximatoin of the light bending, tested our method against exact numerical ray-tracing techniques
- The results are accurate for inclinations **< 80°** or spins **< 0.8;** the method allows fast and flexible computation of polarization spectra and is used to analyse the IXPE observations such as of CygX-1

Contribution of the secondary images

Contribution is less than 0.5% across all cases